Systemic Treatment of Fabry Disease Using a Novel AAV9 Vector Expressing α-Galactosidase A

Maria Grazia Biferi, Mathilde Cohen-Tannoudji, Andrea García-Silva, Olga Souto-Rodríguez, Irene Viéitez-González, Beatriz San-Millán-Tejado, Andrea Fernández-Carrera, Tania Pérez-Márquez, Susana Teijeira-Bautista, Soraya Barrera, et al.

Molecular Therapy
Methods & Clinical Development
Original Article

Systemic Treatment of Fabry Disease Using a Novel AAV9 Vector Expressing α-Galactosidase A

Maria Grazia Biferi,[1] Mathilde Cohen-Tannoudji,[1] Andrea García-Silva,[2] Olga Souto-Rodríguez,[2] Irene Viéitez-González,[2] Beatriz San-Millán-Tejado,[2] Andrea Fernández-Carrera,[2] Tania Pérez-Márquez,[2] Susana Teijeira-Bautista,[2] Soraya Barrera,[2] Vanesa Domínguez,[3,4,5] Thibaut Marais,[1] África González-Fernández,[4,5] Martine Barkats,[1] and Saida Ortolano[2]

[1]Sorbonne Université, INSERM, Institute of Myology, Centre of Research in Myology, 75013 Paris, France; [2]Rare Diseases and Pediatric Medicine Research Group, Galicia Sur Health Research Institute (IIS Galicia Sur), SERGAS-UVIGO, Hospital Álvaro Cunqueiro, 36312 Vigo, Spain; [3]Bioexperimentation Service of the University of Vigo (Sbio), Campus Universitario Lagoas, Marcosende, 36310 Vigo, Spain; [4]CINBIO, Centro de Investigaciones Biomédicas, Universidade de Vigo, Immunology Group, Campus Universitario Lagoas, Marcosende, 36310 Vigo, Spain; [5]Immunology Group, Galicia Sur Health Research Institute (IIS Galicia Sur), SERGAS-UVIGO, Vigo, Spain

Fabry disease is a rare X-linked disorder affecting α-galactosidase A, a rate-limiting enzyme in lysosomal catabolism of glycosphingolipids. Current treatments present important limitations, such as low half-life and limited distribution, which gene therapy can overcome. The aim of this work was to test a novel adeno-associated viral vector, serotype 9 (AAV9), ubiquitously expressing human α-galactosidase A to treat Fabry disease (scAAV9-PGK-GLA). The vector was preliminary tested in newborns of a Fabry disease mouse model. 5 months after treatment, α-galactosidase A activity was detectable in the analyzed tissues, including the central nervous system. Moreover, we tested the vector in adult animals of both sexes at two doses and disease stages (presymptomatic and symptomatic) by single intravenous injection. We found that the exogenous α-galactosidase A was active in peripheral tissues as well as the central nervous system and prevented glycosphingolipid accumulation in treated animals up to 5 months following injection. Antibodies against α-galactosidase A were produced in 9 out of 32 treated animals, although enzyme activity in tissues was not significantly affected. These results demonstrate that scAAV9-PGK-GLA can drive widespread and sustained expression of α-galactosidase A, cross the blood brain barrier after systemic delivery, and reduce pathological signs of the Fabry disease mouse model.

INTRODUCTION

Fabry disease (FD; MIM: 301500) is one of the most frequent lysosomal storage disorders (LSDs), which affects around 1:7,000 individuals, according to several newborn screening studies.[1,2] FD is caused by mutations in *GLA* (NCBI: NC_000023.11; Xq22), which encodes α-galactosidase A (α-GalA; BRENDA: EC3.2.1.22), a rate-limiting enzyme in the lysosomal metabolism of glycosphingolipids. Lack of α-GalA leads to the progressive accumulation of glycosphingolipids, mainly globotriaosylceramide (Gb3), and its deacylated form Lyso-Gb3. Progressive accumulation of glycosphingolipids within lysosomes of FD individuals occurs in a variety of cell types, including endothelial, smooth muscle, and renal cells (podocytes, tubular cells, glomerular endothelial, mesangial, and interstitial cells), as well as cardiac (cardiomyocytes and fibroblasts) and nerve cells. These events cause a progressive multiorgan disorder that manifests with a painful small fiber neuropathy, cardiac disease, chronic renal insufficiency, and a high predisposition for cerebrovascular strokes.[3] FD equally affects males and females because random inactivation of one of the two X chromosomes in females may be sufficient to develop severe manifestations.[4] Up-to-date FD is treated by enzyme replacement therapy (ERT), which consists of biweekly intravenous (i.v.) injections of recombinant human α-GalA (agalsidase alpha or agalsidase beta). This therapeutic approach slows down organ damage, stabilizes renal or cardiac parameters, and reduces neuropathic pain crisis in FD patients.[5] Nonetheless, ERT presents significant limitations for long-term treatment of FD, such as low half-life and biodistribution, activation of the immune system, the inability to cross the blood brain barrier (BBB), and the mode of administration. Recently, a novel orally active chaperone, migalastat HCl, has been approved for FD.[6] Although this drug can achieve therapeutic concentrations in the central nervous system (CNS), its use is only indicated for a fraction of FD patients with amenable mutations in *GLA* (∼70%). Different strategies are currently being developed to increase the efficacy of ERT, including gene therapy and small molecules.[7,8] These therapeutic approaches are based on the evidence that even a modest increase in α-GalA activity could prevent clinical manifestations. Indeed, in several LSDs, substrate accumulation occurs when residual enzyme

Received 13 July 2020; accepted 17 October 2020;
https://doi.org/10.1016/j.omtm.2020.10.016.

Correspondence: Saida Ortolano, PhD, Rare Diseases and Pediatric Medicine, Galicia Sur Health Research Institute, Hospital Álvaro Cunqueiro, Bloque Tecnico, Planta 2 A, Estrada Clara Campoamor 341, 36312 Vigo (Pontevedra), Spain.
E-mail: saida.ortolano@iisgaliciasur.es

activity decays below a threshold (usually activity <10%).[9] The classical form of FD is related to residual α-GalA activity <1% in men, whereas a residual activity of 5%–10% may be sufficient to prevent clinically significant Gb3 accumulation.[10]

In comparison with ERT, adeno-associated viral vector (AAV)-based gene therapy ensures an increased half-life and bioavailability of the enzyme and could be easily directed to specific tissues or even cell types. AAVs are a group of DNA viruses of the *Parvoviridae* family and the *Dependoparvovirus* genus, which are incapable of self-replication and can be easily manipulated to produce recombinant proteins.[11] For these advantages, they are currently, extensively used in gene therapy clinical trials.[12]

AAV1, AAV2, and AAV8 serotypes have been used to express α-GalA in murine models of FD, where they successfully cleared glycosphingolipid storage from peripheral organs.[13–15]

Ogawa et al.[13] used an AAV1 to drive the expression of α-GalA in newborns and adult males of a FD mouse model. AAV1 achieved α-GalA expression in liver, heart, and plasma; however, no effects were observed in adult females.

Ziegler et al.[15] designed hepato-specific targeting to treat FD animal models by combining the AAV8 serotype (with high transduction affinity for the liver) and a liver-restricted promoter (DC190). The local administration of the vector in the liver afforded successful levels of α-GalA even in peripheral organs; in addition, the elevated hepatic concentration of the enzyme induced immunotolerance to the transgene, a favorable feature for possible clinical applications. Site-specific genome editing, providing long-term, stable therapeutic expression from the endogenous promoter in the serum albumin locus, has also been tested.[16] Lastly, a lentiviral vector-based *ex vivo* gene therapy approach for FD is under investigation in clinical trials.[17]

Overall, the major limitation of the methods that have been developed thus far is that they do not allow sufficient expression of α-GalA in the CNS. Although no severe cognitive impairment has been associated to FD, α-GalA is expressed in neurons and glia. Neurologic symptoms are substantial in the pathophysiology of the disease,[18] and stroke at early age is one of the main causes of premature death in FD patients.[19,20]

Therefore, the aim of this work was to develop an efficient vector for the expression of α-GalA in the CNS and peripheral organs of an FD mouse model. Our approach was based on the systemic injection of an AAV9, which demonstrated tropism for nervous tissue and the ability to cross the BBB.[21,22]

We found that systemic administration of the newly generated vector mediated widespread α-GalA expression and restored its function in the CNS and in multiple tissues of a knockout mouse model of FD at both the presymptomatic (at birth and 1 month of age) and symptomatic stages of the disease (at 3 months of age). Furthermore, we demonstrated that the treatment prevented glycosphingolipid accumulation in the most affected tissues (heart, liver, kidney, CNS) by immunofluorescence, ultrastructural examination, and liquid chromatography-mass spectrometry (LC-MS) analysis of either Gb3 or Lyso-Gb3. Interestingly, the therapeutic effect was observed in both males and females and was not reduced even in the presence of a humoral immune response in mice injected at 3 months of age. Our data indicate that this gene therapy is a very promising approach for the translation into treatment protocols for FD.

RESULTS

Injection of Self-Complementary AAV9-Phosphoglycerate Kinase-α-GalA (scAAV9-PGK-GLA) Induces High and Widespread α-GalA Activity *In Vivo*

To efficiently express α-GalA *in vivo*, we produced a novel scAAV9 vector encoding the human α-GalA cDNA (GenBank: NM_000169.3), under the control of the ubiquitous PGK promoter (scAAV9-PGK-GLA). We also generated a similar AAV9 vector, expressing the green fluorescent protein (GFP), used as control (scAAV9-PGK-GFP).

We initially tested the expression of the two vectors in wild-type FVB/NRj mice. To ensure a widespread distribution of the viral particles and detection of α-GalA in multiple organs, we codelivered a high dose of vector (3.2×10^{14} vector genome [vg]/kg) via combined intracerebroventricular (i.c.v.) and i.v. injections at postnatal day 1 (P1), as we previously described.[23] 2 months after treatment, we analyzed α-GalA activity in the brain, spinal cord, heart, kidney, and liver of injected mice. In all tissues of the animals injected with scAAV9-PGK-GLA, the enzymatic activity was significantly higher (14- to 82-fold) compared to noninjected or GFP-treated mice (Figure S1) except in the kidney (5-fold increase). Notably, α-GalA activity was 20-fold higher in the brain and spinal cord of the mice injected with scAAV9-PGK-GLA compared to noninjected or scAAV9-PGK-GFP-treated mice, indicating that the vector gets efficiently expressed in the CNS. This pilot experiment demonstrated that the scAAV9-PGK-GLA was efficient to induce widespread overexpression of a functional α-GalA *in vivo*.

Single i.v. Injection of scAAV9-PGK-GLA Induces Sustained α-GalA Activity and Reduces Gb3 Accumulation in FD Mice Treated at Birth

To test the therapeutic efficacy of the scAAV9-PGK-GLA vector *in vivo*, we used the α-GalA knockout mouse strain *B6;129-Gla^{tm1Kul}/J* (FD mice) in which *Gla* is deleted in the X chromosome.[24] These mice recapitulate FD symptoms, namely the accumulation of glycosphingolipids and abnormal kidney and liver morphology, as well as mild cardiovascular pathology, by 3 months of age. However, they have a mild phenotype and normal lifespan, and do not develop evident movement or behavioral alterations.[25]

The i.v. delivery of scAAV9 vectors has already been approved for gene replacement to treat an infantile form of a rare motor neuron disease.[26,27] For this reason and to facilitate translation into the clinic,

Table 1. Experimental Plan of Treatments in Newborn FD Mice

	Genotype and Treatment			
	Hemizygous (Males)			Wild Type (Males)
Treatment Duration	Noninjected	scAAV9-PGK-GLA (1.8×10^{14} vg/Kg)	scAAV9-PGK-GFP (1.8×10^{14} vg/Kg)	Noninjected
3 months	4 (P1–P3)	4 (P1–P3)	4 (P1–P3)	4 (P1–P3)
5 months	4 (P1–P3)	4 (P1–P3)	4 (P1–P3)	4 (P1–P3)

Mice were injected in the temporal vein with either scAAV9-PGK-GLA or scAAV9-PGK-GFP, using 40 μL of virus solutions at the concentration of 1.3×10^{13} vg/mL in PBS (1.8×10^{14} vg/kg). P, postnatal day.

we chose to test our vector following a single-dose i.v. injection in FD mice. We injected scAAV9-PGK-GLA or control scAAV9-PGK-GFP in the temporal vein of newborn hemizygous FD mice at the dose of 1.8×10^{14} vg/kg. To assess short- and long-term effects of α-GalA expression, we sacrificed FD mice at either 3 or 5 months after injection and compared data obtained in mice treated with scAAV9-PGK-GLA to age-matched positive (wild-type male mice) and negative controls (noninjected or scAAV9-PGK-GFP-injected hemizygous). The experimental plan is presented in Table 1.

We measured α-GalA activity in different organs (brain, spinal cord, liver, heart, and kidney). We found that the human enzyme was expressed and functional 3 and 5 months after injection, with maintained or higher levels of α-GalA activity at 5 rather than at 3 months after injection. Moreover, the enzymatic activity was similar in mice injected with the scAAV9-PGK-GLA and wild-type mice in all of the analyzed tissues. In contrast, residual activity was undetected, either in noninjected hemizygous FD mice or in mice treated with the control vector scAAV9-PGK-GFP (Figure 1). Interestingly, this test in FD mice confirmed that the vector was able to drive transgene expression also in the B6;129 mouse background.

We also assessed the distribution of the glycosphingolipid deposits by immunofluorescence and electron microscopy. The amount of Gb3 storage was lower in the heart, kidney, liver, and brain of animals injected with the scAAV9-PGK-GLA vector compared to noninjected hemizygous FD mice. Specifically, Gb3 deposits, detected by immunohistochemistry, were reduced in intracardiac fibroblasts, vascular smooth muscle cells, endothelial cells, and cells (possibly Kupffer cells) of the hepatic sinusoidal space (Figure 2). Importantly, the ultrastructure of electron-dense, intralysosomal inclusions and multilamellar bodies typical of FD were reduced in the heart (including cardiomyocytes), kidney, and vessels of an injected mouse compared with a nontreated hemizygous (Figures S2 and S3). Consistent with previously reported data, we could not observe intralysosomal inclusions in neurons and hepatocytes of the mice from all of the experimental groups, including the noninjected FD mice (Figure S4).[25] By immunofluorescence, we detected the Gb3 signal (but not lysosomal storage) in the cells of the CNS (Figure S5; cerebellum), where this glycosphingolipid is expressed in neurons of cerebral cortex, hippocampus, and cerebellum, independently of the genotype.[28] The Gb3 signal appeared more intense in nontreated mice compared to 5-month-old wild-type mice, and a partial decrease of signal intensity was detected in mice treated at birth with scAAV9-PGK-GLA after 3 and 5 months. These results demonstrated that the presymptomatic treatment of FD mice with the scAAV9-PGK-GLA vector restores α-GalA activity in both the CNS and peripheral organs for up to 5 months and induces a marked, long-lasting reduction of Gb3 deposits in multiple organs of FD mice.

Systemic Injection of scAAV9-PGK-GLA Preserves Body Weight of Adult FD Mice of Both Sexes, Treated at the Presymptomatic and Symptomatic Stages

The encouraging results observed in the newborn animals prompted us to test the scAAV9-PGK-GLA vector in adult FD mice at two different stages of the disease (1 month of age, presymptomatic; or 3 months of age, presenting clinical symptoms).

We performed a comprehensive analysis of the effects induced by the scAAV9-PGK-GLA systemic injection in adult FD mice.

To evaluate a dose-response effect, we tested two vector doses: 6×10^{13} vg/kg and 1.8×10^{14} vg/kg. For a complete therapeutic assessment, we also included heterozygous females in which *Gla* is knocked out in one allele, as shown in the experimental plan presented in Table 2. The use of heterozygous female mice instead of homozygous is clinically relevant because women FD patients are usually heterozygous.

We monitored mice weekly for health conditions and body weight over a period of 5 months after treatment. The body weight analysis did not reveal any significant effect of the treatment on the growth of FD mice (Figure S6), with no difference in body weight in treated or untreated FD mice versus wild-type mice (mixed ANOVA). This indicates that the FD mouse model does not present growth defects when compared to wild-type mice over the first 8 months of age and suggests that the treatment was well tolerated.

Although the hemizygous mice, injected at 1 month of age with the highest dose, had a lower starting body weight compared to the animals of the same age in the other experimental groups, the rate of weight increase in this group was comparable with the one registered in the remaining groups ($p = 0.191$, ANOVA). This confirms a lack of impact of the gene therapy on FD mouse growth.

Survival was unaffected in all treated mice, and no phenotype alteration was noticed during the study, confirming the lack of a severe phenotype in FD mice.[25] Both treated and untreated FD mice were slightly more aggressive than wild-type animals. This could be explained by the presence of sensorimotor function alteration, similarly to the human pathology. However, this symptom tends to disappear over time in both humans and mice, due to progressive nerve-ending degeneration, caused by Gb3 accumulation.[29,30] In general anxiety, depression, and cognitive symptoms, which are frequently described in FD patients, have a subordinate relevance in the mouse model.[31]

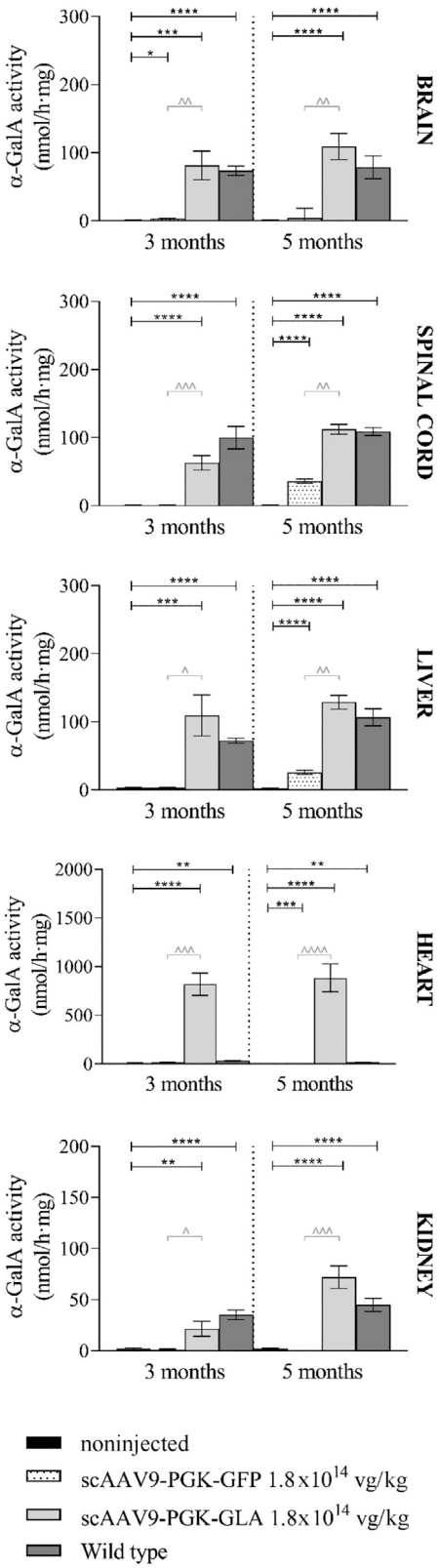

Figure 1. Activity of α-GalA Is Restored in FD Hemizygous Newborns Injected with the scAAV9-PGK-GLA

Histograms represent α-GalA activity (nmol/hour × mg), measured at the study end point, in the indicated tissues (brain, spinal cord, liver, heart, kidney) from hemizygous FD mice treated at birth with either scAAV9-PGK-GLA or scAAV9PGK-GFP and noninjected hemizygous (negative control) or wild-type (positive control) mice. Data were collected 3 or 5 months after injection. Values are expressed as the mean ± standard error of the mean (SEM). Statistical significance was assessed by nonparametric t test comparing animals treated with scAAV9-PGK-GLA to noninjected animals (*$p < 0.05$; **$p < 0.01$; ***$p < 0.001$; ****$p < 0.0001$) or to animals treated with scAAV9-PGK-GFP (^$p < 0.05$; ^^$p < 0.01$; ^^^$p < 0.001$; ^^^^$p < 0.0001$).

Systemic Injection of scAAV9-PGK-GLA Induces Expression of a Functional α-GalA in Multiple Tissues of Adult FD Mice, Including the Brain

To assess to what extent the scAAV9-PGK-GLA was able to target different tissues, we titered vector particles in tissues 5 months after injection, by droplet digital PCR (ddPCR), using specific primers for scAAV9 genome. We detected scAAV9-PGK-GLA in the brain, heart, liver, and kidney of mice injected at 1 month and 3 months of age, at a concentration ranging between 11 and 2,120 vg per diploid genome (dg; Figure 3A). The highest transduced organ was the liver (ranging from 757 to 2,120 vg/dg), whereas the brain was the organ with the lowest absolute quantification of viral particles (ranging from 11 to 75.4 vg/dg). Viral vector concentrations in the different tissues were comparable between mice injected at 1 month or 3 months of age, since differences (nonparametric t test) between groups with the same sex and treatment, at the two different ages, were not statistically significant. This suggests that equal amounts of vector reached the tissues independently of the stage of the disease. Despite that vector dose was adjusted to mice weight, it appeared that the transduction of the BBB was more efficient when mice were injected at a younger age (1 month). Viral vector titer in tissues tends to be higher in animals treated with the higher dose of the vector, although differences among the groups did not reach statistical significance.

To analyze whether the scAAV9-PGK-GLA induced enzyme expression in different organs of FD mice, we assessed α-GalA expression by western blot (WB) in brain, liver, heart, kidney, and plasma samples from treated and nontreated FD mice. The enzyme was expressed in all of the analyzed tissues from treated animals injected at either 1 month or 3 months of age (Figures 3B, 4, S7, and S8) compared to nontreated FD mice. Plasmatic protein levels were variable among animals, and in 12 out of 32 of the analyzed samples, α-GalA was barely detectable (Figure S7).

To evaluate whether the replaced enzyme was functional, we assessed specific α-GalA activity in plasma and tissue samples (brain, spinal cord, liver, heart, and kidney) of all groups at the study end point (Figure 5).

Similarly to what we observed in newborn mice, the α-GalA was functional and in all analyzed tissues of the adult animals that were injected with scAAV9-PGK-GLA vector. Consistently with WB results, activity in plasma was variable.

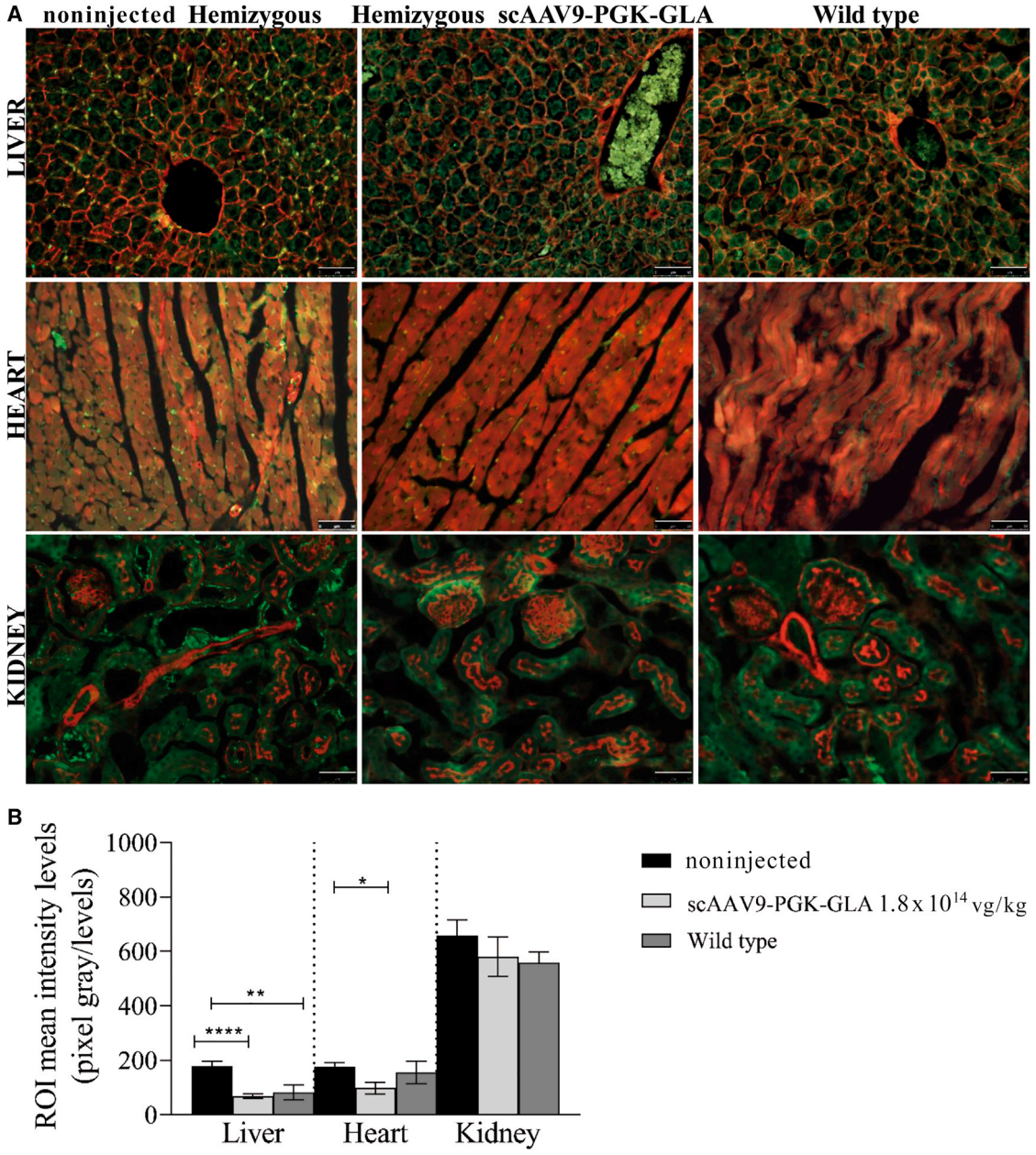

Figure 2. Gb3 Deposits Are Reduced in Tissues from Hemizygous FD Mice after Treatment with scAAV9-PGK-GLA

(A) Representative immunofluorescence images of Gb3 deposits in tissues from newborn hemizygous mice injected with scAAV9-PGK-GLA. The same analysis was performed in age-matched controls (noninjected hemizygous and wild-type mice). Gb3 deposits were detected with an anti-Gb3 antibody (green); polymerized actin was marked with anti-phalloidin-rhodamine (red). Heart, liver, and kidney tissues collected 3 months after injection. Scale bars, 50 μm. (B) Histograms representing mean fluorescence in green channel (mean pixel intensity) as computed in different regions of interest (ROIs), with constant area, defined for each image in (A). Error is expressed as SEM. Significance of the data, comparing each value with the value of the corresponding noninjected control, was assessed by nonparametric t test (*$p < 0.05$; **$p < 0.01$; ***$p < 0.001$).

Importantly, the levels of enzyme activity in the brain and spinal cord of the adult hemizygous-treated animals ranged between 10% and 30% of physiological activity (noninjected wild-type FD males) in the same organs. Heterozygous-treated animals presented enzyme levels in the CNS comparable to those of noninjected wild-type FD females.

We also found that when we injected the mice at 1 month of age (in the presymptomatic phase), the activity levels increased with the dose, whereas this was not always the case when animals were injected at 3 months of age, consistently with the appearance of cell damage at this stage.

Table 2. Experimental Plan of Treatments in Adult FD Mice

5 Months Follow-Up					
Age of Injection	Injected with scAAV9-PGK-GLA		Noninjected Controls		
	Dose (6×10^{13} vg/kg)	Dose (1.8×10^{14} vg/kg)	Hemizygous	Heterozygous	Wild Type
1 month	4 hemizygous, 4 heterozygous	4 hemizygous, 4 heterozygous	4 males	4 females	4 males, 4 females
3 months	4 hemizygous, 4 heterozygous	4 hemizygous, 4 heterozygous	4 males	4 females	4 males, 4 females

Mice were injected in the tail vein with a solution of scAAV9-PGK-GLA at the concentration of 3.13×10^{13} vg/mL in PBS, adjusting the injected volume to the weight of the mice, to obtain a final dose of either 6×10^{13} vg/kg or 1.8×10^{14} vg/kg.

To analyze the interdependence of the variables (activity, protein levels, and viral titer), we calculated Spearman's rank correlation coefficient (Rho; Table S1) using data obtained in plasma and tissue samples derived from organs that were evenly and consistently cut in fragments and lysed with the appropriate protocol.

Plasmatic α-GalA levels and activity tendentially correlated in samples from the treated hemizygous mice. The presence of the endogenous allele likely impacted a potential correlation between the two variables in heterozygous mice (Figure S9).

Viral particles distribution (assessed by ddPCR), exogenous protein expression (WB data), and α-GalA activity, among the different organs, were consistently higher in injected mice compared to noninjected FD mice, but we did not find a significant correlation among these three variables. However, we observed that in several of the assessed conditions, Rho value was higher than 0.7 (correlated variables), and in the case of heterozygous mice injected with the lower dose, correlation between virus titer and activity in the liver was close to significance ($p = 0.051$).

Overall, we demonstrated that scAAV9-PGK-GLA induces the expression of functional α-GalA in adult FD mice, and the efficacy of the treatment is higher when this is applied before the appearance of the symptoms.

scAAV9-PGK-GLA Mediates Expression of α-GalA-Reduced Glycosphingolipid Deposits in Adult FD Mice

To assess whether FD symptoms were reversed by scAAV9-PGK-GLA injection, we also analyzed levels of the major Gb3 circulating metabolite, Lyso-Gb3, in plasma (before injection, as well as 4 months and 5 months after treatment) and in tissues (brain, liver, heart, and kidney) by LC-MS.

Although Lyso-Gb3 levels in plasma tended to increase over time in nontreated mice, they were dramatically reduced in the mice injected with scAAV9-PGK-GLA (Figure 6). Lyso-Gb3 concentration was significantly decreased in treated hemizygous mice injected at 1 month ($p < 0.0001$) and at 3 months ($p < 0.001$) for each time and dose, as well as in heterozygous mice injected at 1 month ($p < 0.05$ for each time and dose) compared to noninjected genotype-matched mice. In heterozygous FD mice injected at 3 months, the p value of Lyso-Gb3 decrease is <0.05, 4 months after injection, and $p < 0.09$ (6×10^{13} vg/kg) or $p < 0.06$ (1.8×10^{14} vg/kg), 5 months after injection, compared to nontreated FD heterozygous. Plasma Lyso-Gb3 concentration in noninjected FD heterozygous was about 10-fold lower compared to the one in noninjected hemizygous. This may explain why the difference in Lyso-Gb3 concentration between treated heterozygous and nontreated animals is smaller and therefore not statistically significant in all of the assessed conditions. This is not surprising, since the low concentration of Lyso-Gb3 in plasma of female human patients is one of the main limitations in which to consider Lyso-Gb3 as an optimal biomarker for FD diagnosis.[32]

Similarly, Lyso-Gb3 concentration in the tissues of the treated FD mice was significantly lower compared to the levels found in nontreated genotype-matching animals.

This was in line with what we observed in the immunohistochemistry experiments. Gb3 deposits were detectable in the same cell types described for the newborn-injected mice (i.e., intracardiac fibroblasts, renal epithelial tubular cells, vascular smooth muscle cells, endothelial cells, Kupffer cells; Figures 7A and S10). Moreover, we observed an intense Gb3-positive signal in the bone (osteoblasts and bone marrow cells) and the neurons of the dorsal root ganglia in spinal cord sections from noninjected FD hemizygous mice, which was considerably decreased in the same cells of FD mice treated at 3 months of age with both doses of the virus (Figures 7B and S11). In the brain, deposits are mainly detectable in blood vessels of nontreated FD mice and are partially cleared in the same mice after injection with scAAV9-PGK-GLA (Figure S12; showing hippocampus and cortex).

These results denote that the exogenous α-GalA is able to reverse the pathological signs of the FD model.

The Detected Humoral Immune Response to α-GalA Does Not Affect Enzyme Activity in Tissues of Injected FD Mice

Lastly, we analyzed whether the injection with the scAAV9-PGK-GLA induced the production of immunoglobulin G (IgG) antibodies against α-GalA, which may neutralize the action of the enzyme. We found that 9 out of 32 injected animals (28.1%) produced IgG antibodies against human α-GalA in relevant concentrations (Figure 8).

Six of these mice were injected at 3 months of age during the symptomatic phase. Moreover, the activity in plasma was lower than average in samples from all of the animals injected at 3 months and

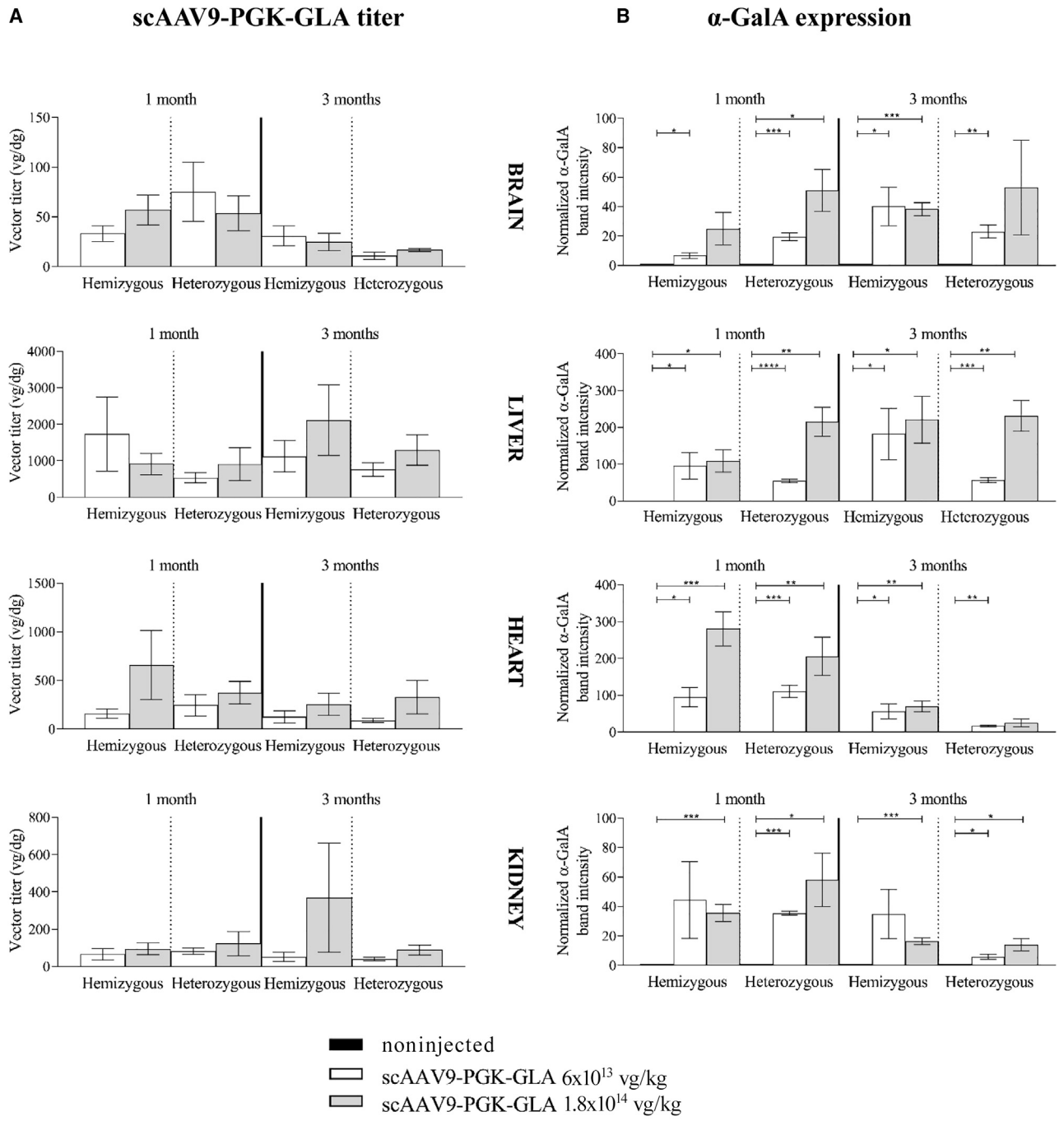

Figure 3. Viral Vector Is Distributed in Tissues of Presymptomatic and Symptomatic FD Mice and Drove the Expression of α-GalA after Systemic Injection

(A) Histograms of viral titer (vg/dg) assessed by ddPCR absolute quantification in different tissues (brain, heart, liver, and kidney) from mice of both sexes injected with scAAV9-PGK-GLA at either 1 month or 3 months of age and sacrificed 5 months later. Measurements were carried out in duplicate samples for each mouse of the group (N = 4). Error is expressed as SEM. Data were compared using nonparametric t test. (B) Histograms of western blot densitometric analysis of α-GalA, normalized to the corresponding total protein per lane (Figure S8) and reported to the intensity value obtained for the corresponding noninjected control. Error is expressed as SEM. Significance of the data, comparing each value with the value of the corresponding noninjected control, was assessed by nonparametric t test (*$p < 0.05$; **$p < 0.01$; ***$p < 0.001$).

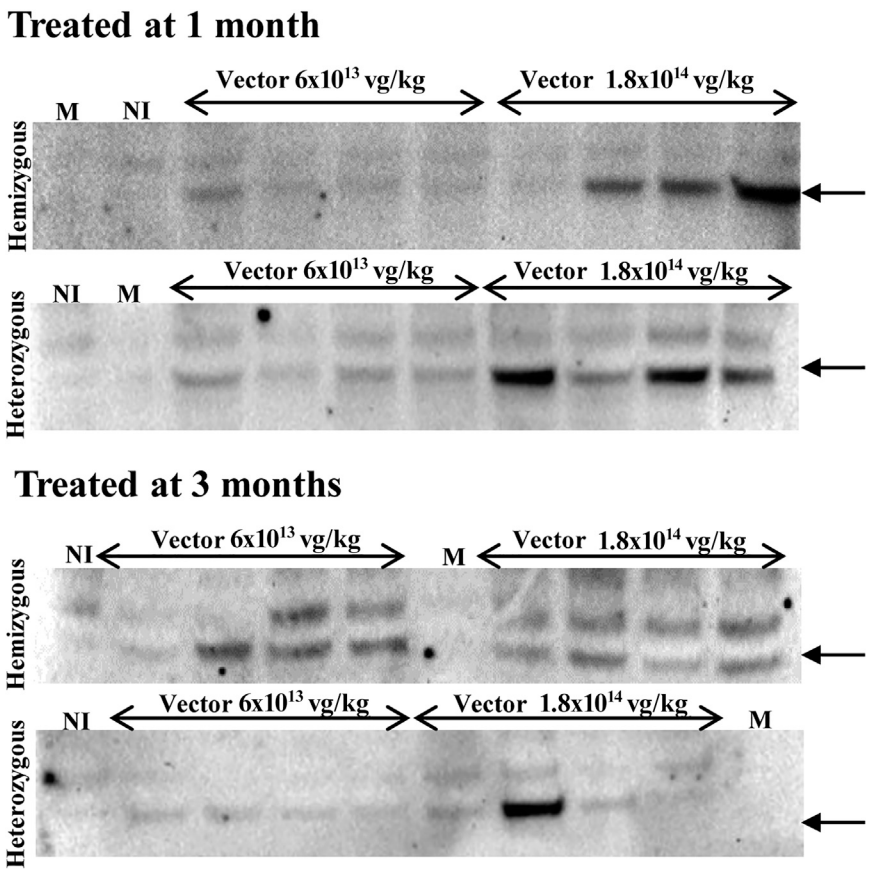

Figure 4. α-GalA Protein Is Expressed in the Brain of Adult FD Mice, Injected with scAAV9-PGK-GLA

Western blot of brain tissues from 4 mice injected with scAAV9-PGK-GLA at either 1 month or 3 months of age with 6×10^{13} or 1.8×10^{14} vg/kg of vector. Tissue was collected 5 months following the injection. A primary antibody, specific for the human isoform, was used to detect α-GalA. NI represents noninjected control. In the remaining lanes, samples were obtained from each one of the treated mice at the indicated conditions (N = 4 per group). Specific human α-GalA band (indicated with a black arrow) was present in all brain samples from treated mice independently of the dose or the age. A nonspecific band of higher molecular weight, which is absent in western blot analysis of the liver (Figure S7), was also detected in all samples.

two of the animals injected at 1 month (presymptomatic) that produced anti-α-GalA antibodies (Table S2). This suggests higher immunological tolerance in presymptomatic mice (81% of the animals) compared to symptomatic mice (44%). Although low enzymatic activity in plasma of treated FD mice tended to correlate with low levels of the protein in plasma, a neutralizing effect of the activity due to the presence of anti-α-GalA antibodies cannot be excluded.

Nevertheless, α-GalA activity was not significantly affected in the analyzed tissues from mice that produced IgG antibodies. Indeed, activity in the liver, brain, heart, and kidney from mice that produced IgG antibodies against α-GalA was comparable or higher than the average activity of the whole group in each tested condition. Only in the spleen, which is directly involved in IgG production, did we detected decreased enzymatic activity (34%–86% of average) in anti-α-GalA IgG-producing mice (Table S2). Thus, these results suggest that despite the possible presence of neutralizing antibodies, the therapeutic effect of the treatment is maintained, since levels of α-GalA activity in tissues are similar to the ones found in mice that do not produce anti-α-GalA IgGs.

Further studies will be necessary to fully evaluate the extent of the immune response and the significance for the clinical translation of this vector.

DISCUSSION

In this proof-of-concept study, we generated and fully characterized a novel AAV vector for *in vivo* delivery of α-GalA as an efficacious treatment for FD. Through a single i.v. injection of an α-GalA-expressing scAAV9, we were able to observe therapeutic effects in a well-established mouse model of FD. We demonstrated that scAAV9-PGK-GLA was able to efficiently express human α-GalA in both the CNS and peripheral organs of FD newborn and adult mice. The human enzyme was functional and reached sufficient levels to mediate a beneficial effect in either hemizygous or heterozygous FD mice at both presymptomatic and symptomatic stages. Indeed, after treatment, Lyso-Gb3 levels, which inversely correlate with α-GalA, were almost null in plasma and multiple tissues (including the CNS) of FD mice treated with scAAV9-PGK-GLA compared to nontreated FD mice.

CNS targeting represents a major advancement for FD treatment, since currently developed therapies fail to rescue pathological signs in the brain. Among the treatments in use, ERT is not able to reach the CNS, and migalastat, which can diffuse through the BBB, is not indicated for all patients. Although FD is mostly considered a pathology with peripheral and cardiovascular implications, we believe that the expression of α-GalA in the CNS of FD patients has a therapeutic value, especially when this is reached using noninvasive methods. α-GalA is normally present in different cell types of the brain, whereas glycosphingolipid inclusions have been observed in neurons, Schwann cells, perineural cells, dorsal root ganglia, and autonomic ganglia in FD patients, leading to CNS and peripheral nervous system pathology.[33,34] Neurological symptoms are important for patients who very frequently experience neuropathic pain, depression, anxiety, and stroke at an early age, as well as white matter damage. Moreover, a recent study also suggests a possible link between FD and Parkinson's disease.[35]

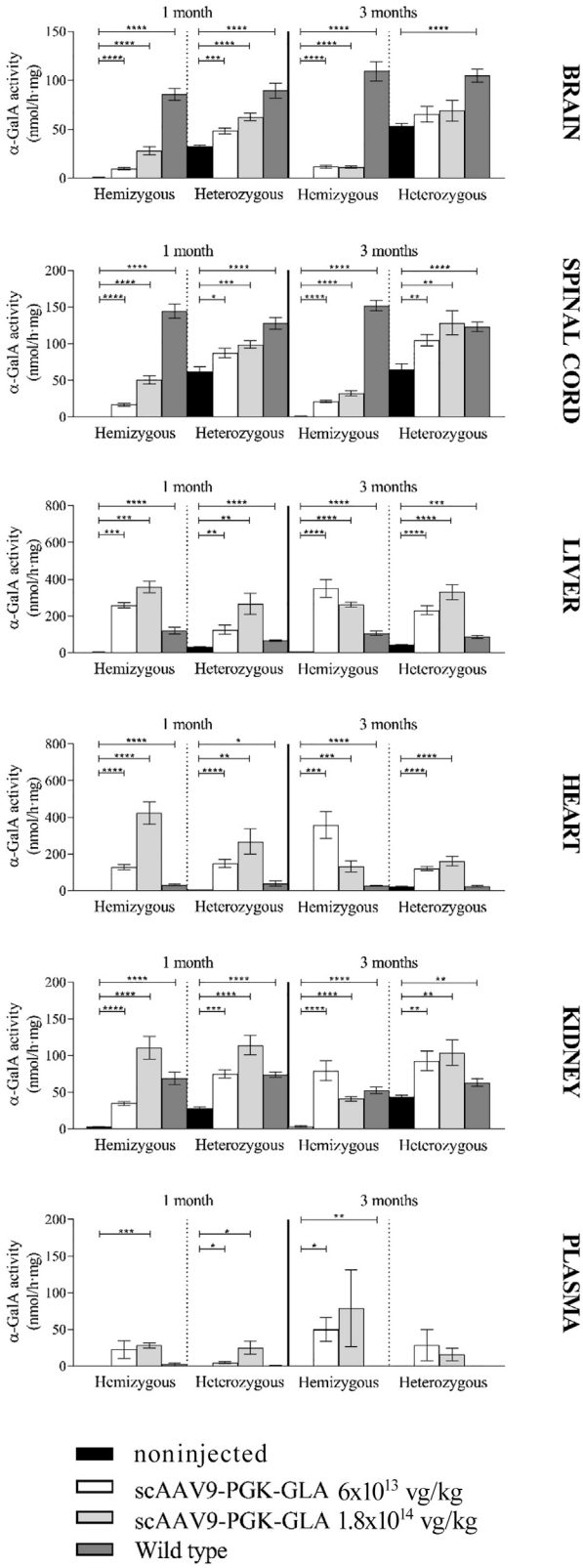

Figure 5. Activity of α-GalA Is Restored in FD Mice Treated with scAAV9-PGK-GLA at Presymptomatic and Symptomatic Stages

Activity of α-GalA (nmol/hour × mg) was measured 5 months after injection in brain, spinal cord, liver, heart, kidney, and plasma samples from FD mice. Activity values from mice injected with scAAV9-PGK-GLA, at either 1 month or 3 months of age, were compared with values obtained in noninjected (negative controls) or wild-type (positive controls) mice. Values are expressed as the mean ± SEM. Statistical significance of the differences between treated mice and noninjected controls was analyzed by nonparametric t test (*$p < 0.05$; **$p < 0.01$; ***$p < 0.001$; ****$p < 0.0001$).

Other gene therapy-based treatments, which target mainly peripheral organs or the liver, are in development for FD; however, none of them is focused on the neurological effects of the protein.

Ex vivo gene therapy approaches with lentiviral vector-mediated correction of a *GLA* genetic defect in $CD34^+$ hematopoietic stem cells and endogenous cell transplantation are currently being tested in clinical trials.[17] However, preclinical data did not assess the expression of α-GalA in the CNS. In addition, *ex vivo* gene therapy has some constraints that are generally related to the percentage of engrafted cells and sustainability of the transgene expression.

In vivo gene therapy, based on direct injection of viral vectors, allows sustained expression of the α-GalA and represents an advantage over ERT. For instance, Ziegler and coworkers[15,36] tested a hepatocyte-specific AAV8 vector achieving long-lasting α-GalA expression in FD mice and nonhuman primates. The main advantage of liver-specific gene therapy relies on its low immunogenicity, since this approach facilitates the development of tolerance. Liver-specific expression of *GLA* is also achieved by the injection of ST-920, an AAV2/6-based vector that reaches supraphysiological levels of α-GalA in plasma and peripheral tissues without safety issues at the preclinical stage.[37] Nonetheless, these strategies behave like an improved ERT, since the recombinant protein is specifically produced in the liver and distributed to other tissues, but it cannot be expressed in the CNS.

Similar to our vector, the construct tested by Ogawa et al.[13] also drives the expression of α-GalA through a ubiquitous promoter (CAG). However, unlike scAAV9-PGK-GLA, their vector was not able to reach a significant increase of α-GalA in FD females' organs nor the CNS. Indeed, Ogawa et al.'s[13] vector preferentially drives α-GalA expression in the liver and to a lesser extent, in the heart of hemizygous adult mice. On the contrary, we demonstrated that our novel vector scAAV9-PGK-GLA is able to transduce tissues and brain of the adult FD mice, independently of sex, leading to increased α-GalA activity in peripheral organs (liver, heart, and kidney), as well as the CNS of FD-treated mice versus untreated mice of the same strain. Therefore, the expressed α-GalA is functional and is able to cross the BBB, with highest levels measured in FD mice injected at the presymptomatic stage.

AAV9 was successfully used to develop gene therapy vectors in other lysosomal disorders, such as the mucopolysaccharidosis I, II, and III.[38–40] Specifically, intrathecal cervical AAV9 gene transfer of

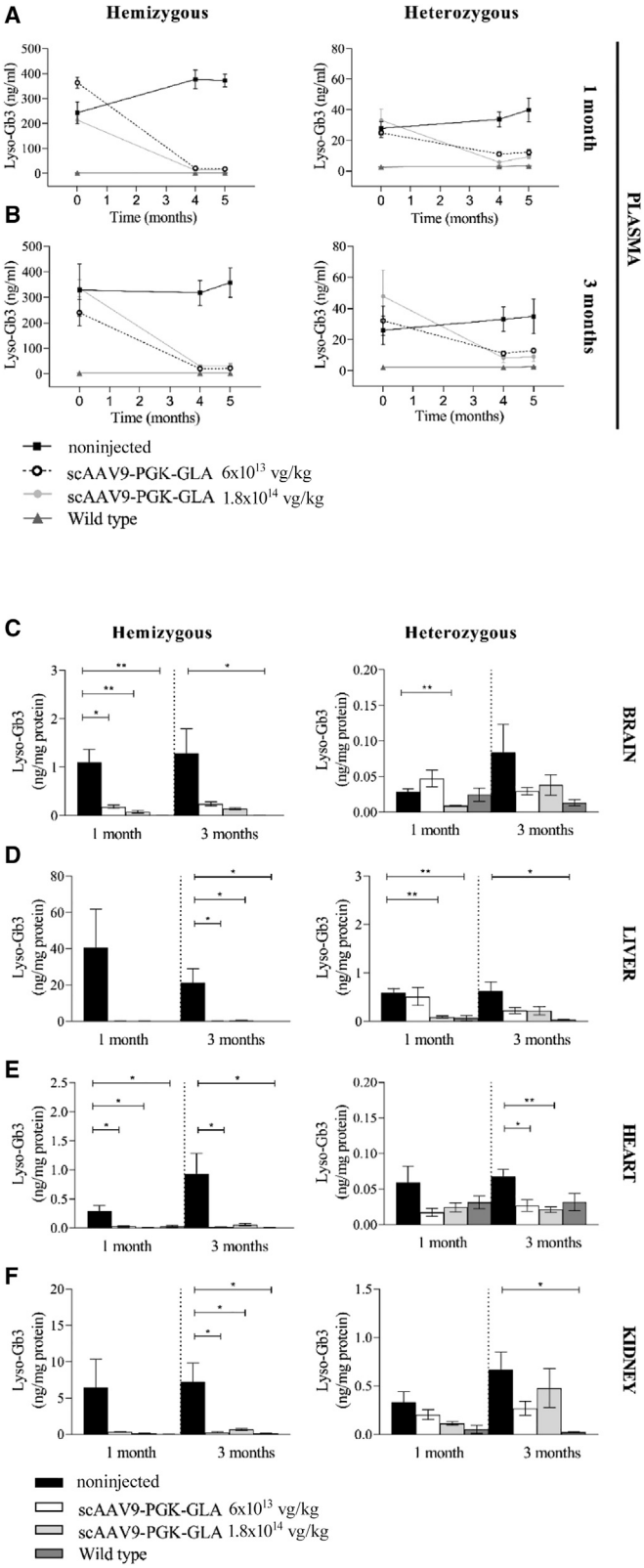

Figure 6. Lyso-Gb3 Concentration Is Reduced in Plasma and Tissues of Adult FD Mice Injected with scAAV9-PGK-GLA

(A and B) Plasmatic concentration of Lyso-Gb3 (ng/mL), assessed by LC-MS in samples obtained before the injection of the virus and 4 or 5 months after injection. Mice were injected at 1 month or 3 months of age. Values were measured in mice treated with scAAV9-PGK-GLA at the two different doses and in age- and sex-matched noninjected FD mice or wild-type controls. Bars represent SEM. (C–F) Lyso-Gb3 concentration (ng/mg of proteins in tissue extracts) assessed in the brain (C), liver (D), heart (E), and kidney (F) of FD mice injected with scAAV9-PGK-GLA and noninjected controls (hemizygous, heterozygous, or wild types of both sexes), 5 months after treatment, mean values. Bars represent SEM, and significance of the differences between treated mice and noninjected hemizygous or heterozygous controls was assessed by nonparametric t test (*$p < 0.05$; **$p < 0.01$; ***$p < 0.001$; ****$p < 0.0001$).

human α-L-iduronidase administered to 1-month-old rhesus monkeys supports the safety and efficiency of the treatment in these animals, even when they were tolerized to the human transgene at birth via systemic administration of an AAV8 vector. The AAV9 expressing α-L-iduronidase efficiently transduced pyramidal neurons in the cortex and hippocampus, Purkinje cells in the cerebellum, lower motor neurons, and dorsal root ganglia neurons.

Systemic injection of scAAV9-PGK-GLA in FD mice produced levels of α-GalA activity in the CNS of about 30% of the physiologic activity (wild-type controls); this finding is clinically relevant because 10% residual enzymatic activity is known to be sufficient to prevent glycosphingolipid accumulation and the development of symptoms in FD patients.[10] Moreover, the vector demonstrated a very high capacity to transduce CNS cells (α-GalA activity increased up to 20-fold) when we administered it through combined i.v. and i.c.v. injection in FVB/NRj newborn mice.

Overall, to the best of our knowledge, our newly developed scAAV9-PGK-GLA is the first vector to enable sustained therapeutic levels of α-GalA in the CNS, through a systemic injection. Therefore, it could be intended as a viable alternative or as a complement for other successfully developed gene therapy approaches when elevated levels of gene expression are needed in the CNS.

Importantly, multiple complementary approaches (LC-MS, immunofluorescence, and ultrastructural examination) demonstrated that glycosphingolipid accumulation was decreased after scAAV9-PGK-GLA treatment, and deposits were mostly cleared in a variety of cell types of injected FD mice. Interestingly, the distribution of Gb3 deposits in tissues from FD mice does not completely resemble the pattern found in FD classical patients, whereas it mimics mainly the histological features of late-onset FD patients.[25] Indeed, podocytes are minimally or nonaffected by the presence of Gb3 storage, which accumulates in epithelial cells of collecting ducts and distal tubules or in vascular smooth muscles and interstitial fibroblasts of the heart, as confirmed by our results (Figures 2, 7A, S2, S3, and S10). However, unlike Bangari et al.[25], we were also able to detect electron-dense, intralysosomal inclusions in a small percentage (~5%–10%) of cardiomyocytes and endothelial cells of the noninjected hemizygous mice, in which formation was prevented by treatment with scAAV9-PGK-GLA (Figures S2E and S2F).

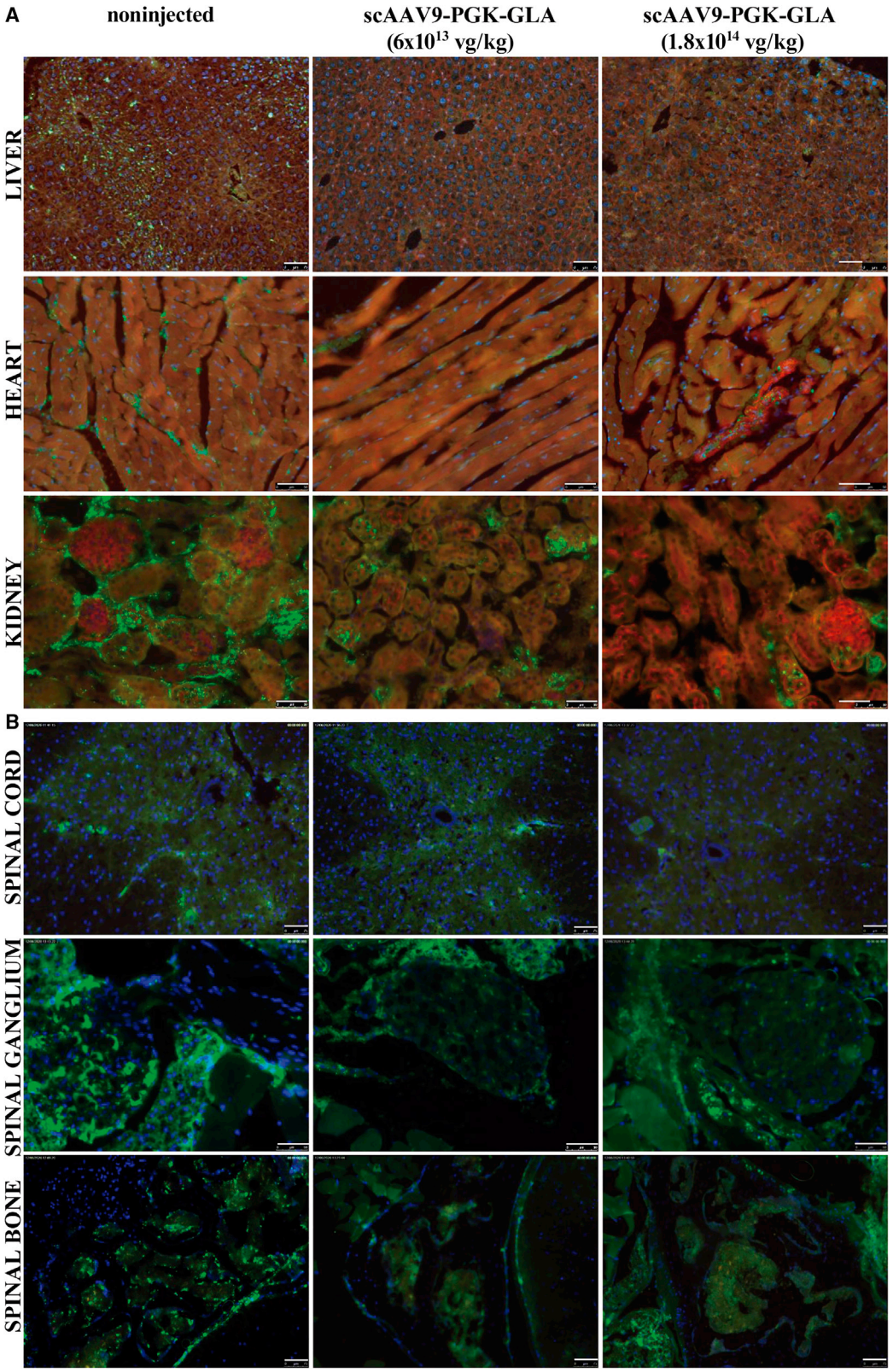

(legend on next page)

Furthermore, in contrast with human pathology, classical multilamellar body accumulation was not described in hepatocytes and brain neurons of hemizygous FD mice, whereas affected neurons were only found in the sensory region of dorsal root ganglia.[25] In accordance with these findings, glycosphingolipid deposits were considerably decreased by the scAAV9-PGK-GLA treatment in neurons of the dorsal root ganglia of hemizygous FD mice (Figure 7B), but we did not observe electron-dense, intralysosomal inclusions, characteristic of FD, in brain neurons and hepatocytes of nontreated FD hemizygous mice (Figure S4). However, we could detect a Gb3-positive signal in the brain by immunohistochemistry (Figures S5, S10, and S12), consistently with the fact that these glycosphingolipids are normally present in the brain of C57BL/6J mice, and the intensity of the signal is partially reduced by the treatment with scAAV9-PGK-GLA in the FD model.[28] These data were also supported by the LC-MS detection of increasing concentrations of Lyso-Gb3 in the brain of nontreated hemizygous and heterozygous FD mice overtime, which are prevented by the treatment that we applied (Figure 6).

Notably, scAAV9-PGK-GLA was effective in reducing Gb3 storage in osteoblasts and bone marrow cells of FD mice (Figure 7B). This finding is important for the translational application of the vector, as it strongly supports the potential of AVV9-based gene therapy for the treatment of LSDs other than FD, such as Gaucher disease and mucopolysaccharidoses, in which bone involvement is a major problem.[41,42]

Our data also demonstrate that the systemic injection of a scAAV9 vector mediates a sustained expression of α-GalA over time, rescuing the FD pathological signs up to 5 months after treatment in mice. This is not surprising, because AAV9 vectors are known to mediate long-lasting expression of transgene under different settings, including mouse models[43] and patients.[44] However, here, we report evidence of the prolonged and widespread effect of such an approach for FD, including the CNS, thereby opening a concrete perspective for the translational application of this vector. Specific experiments will have to be performed to assess safety issues related to α-GalA overexpression, although the general health condition of the animals and the survival data suggest that the enzyme levels are well tolerated.

α-GalA activity data were in accordance with the distribution of the viral particles and the expression of the protein among the different tissues, even though we did not find a significant correlation among the three variables. In plasma, there is a clear tendency of the activity to correlate with the levels of α-GalA in samples from the treated hemizygous mice, which is also evident in mice that produce antibodies against the enzyme. Indeed, IgG antibodies against the α-GalA were produced in 9 out of 32 injected mice with plasmatic activity lower than the average of the group. Although reduced activity correlates with low levels of plasmatic protein, we cannot exclude that the anti-α-GalA antibodies neutralize the activity of the enzyme in plasma, since the enzyme-antibody complexes could have been removed from the circulation by macrophage action. However, the production of IgGs against α-GalA did not seem to affect the functionality of the enzyme in tissues, since activity values in organs from IgG-producing mice were not significantly different from the average value of the group. In particular, animals that were treated at the earlier stage of the disease (1 month, presymptomatic) were less prone to produce antibodies against the enzyme and also showed a more robust dose-response effect. On the contrary, mice treated at 3 months, when Gb3 was already substantially accumulated in the organs, more frequently produced IgG antibodies against the enzyme and did not show a correlation between the enzymatic activity and the administered vector dose. We believe that the poor dose-response correlation in the scAAV9-PGK-GLA-treated FD mice at 3 months of age could be due to a combination of factors, including both pre-existing tissue damage and immune response.

In contrast, the treatment with scAAV9-PGK-GLA in pups with the highest dose of the virus (1.8×10^{14} vg/kg) resulted in high production of functional α-GalA in all analyzed organs. In these initial studies, we did not assess the immune response due to the immaturity of the newborn immune system and the presence of maternal antibodies that inhibit newborn antibody production. During this phase, the immune system is not fully developed, and foreign elements can be more easily tolerated.[45,46] Thus, the AAV administration to newborns could facilitate an immune tolerance to the transgene products.

Importantly, functional α-GalA was expressed in the brain of all the AAV-treated pups, as the transduction across the BBB was more efficient in newborns than in the adult-injected mice, most likely related to the higher permeability of the barrier at this age. Overall, our findings support the conclusion that an early administration of scAAV9-PGK-GLA will result in higher therapeutic efficacy, similar to currently used treatments in FD (ERT or chaperones).

Further studies will be necessary to reduce immunogenicity of the vector, other than applying the treatment at an early age in the presymptomatic stage. For example, local intraventricular injection in the brain could be used to reduce adaptive immune response and widespread expression of the transgene. This delivery route could be used in combination with a treatment that is excluded by the CNS. However, systemic application will more likely lead to a better compliance of the patients, and therefore, early stage treatment

Figure 7. Gb3 Deposits Are Reduced in Tissues from Adult Hemizygous Mice Injected at 3 Months of Age with scAAV9-PGK-GLA

Representative immunofluorescence images of Gb3 deposit in tissues from hemizygous FD mice injected with two doses of scAAV9-PGK-GLA at the age of 3 month and their age-matched, noninjected controls. Mice were sacrificed 5 months after injection. Gb3 was detected with a CD77-fluorescein isothiocyanate (FITC) antibody (green), polymerized actin was stained with phalloidin-rhodamine (red), and nuclei were stained with DAPI (4',6-diamidino-2-phenylindol,blue). (A and B) Peripheral organs (liver, heart, and kidney) (A) andspinal cord, a dorsal root ganglion, and the spinal bone (B) . In heart and ganglion, scale bars, 50 μm; in the remaining images, scale bars, 75 μm. Mean fluorescence in the green channel (mean pixel intensity) was computed in different regions of interest for each image, and it is shown in Figure S11.

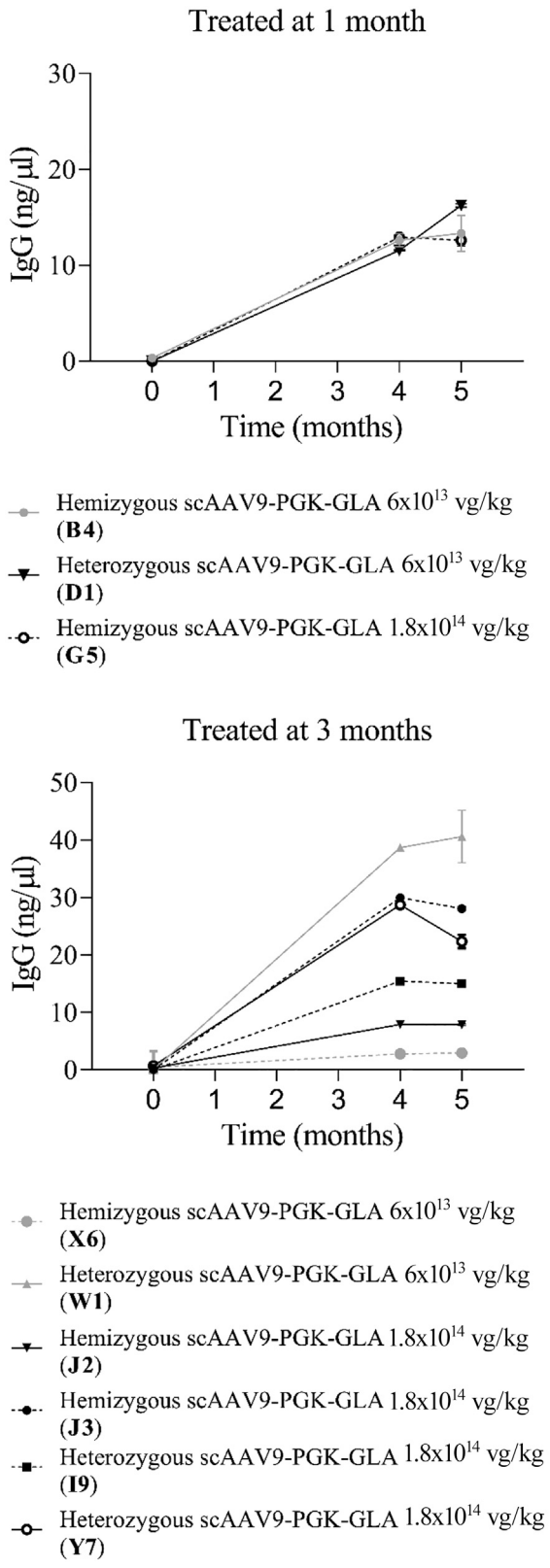

Figure 8. IgG Antibodies against α-GalA Can Be Detected in Plasma from 9 FD Mice Injected with scAAV9-PGK-GLA

(Top) Concentration of IgG antibodies against α-GalA (ng/mL), assessed by ELISA, in plasma samples from 3 FD mice (#B4, D1, and G5), injected at 1 month of age with the indicated dose of scAAV9-PGK-GLA. (Bottom) Concentration of IgG antibodies against human α-GalA (ng/mL), assessed by ELISA, in plasma samples from 6 FD mice (#W1, J2, J3, I9, X6, and Y7), injected at 3 months of age with the indicated doses of the viral vector. In both panels, samples were obtained before injection and 4 and 5 months after the injection. Values are expressed as mean ± SEM (measurements in duplicates).

should be prioritized to reach immunotolerance in a pathology like FD with limited damage in the CNS.

When envisioning systemic delivery of AAV9 vectors as treatment for human diseases, several aspects need to be considered to avoid immune-mediated toxicity that would lead to deaths in clinical trials, as recently reported.[47] Attention must be taken in preclinical studies regarding dose, immune response, and toxicity.

In conclusion, our work demonstrates that the scAAV9-PGK-GLA vector could be a novel potential therapy to treat systemic as well as neurological manifestations of FD. This vector was able to successfully rescue the pathological phenotype of a mouse model of FD when it was injected in the blood circulation of newborns and presymptomatic and symptomatic animals. Given that the standard of care, ERT, does not reach the CNS, and chaperone therapy is indicated for a restricted group of patients, the proposed gene therapy vector represents a promising preclinical therapeutic candidate for FD, which overcomes most of the limitations of currently used approaches.

MATERIALS AND METHODS

Vector Cloning

Human α-GalA cDNA (GenBank: NM_000169.3) was amplified using Phusion High-Fidelity DNA polymerase (F532; Thermo Scientific) from the pR-M10-α-GalA plasmid,[48] and GFP was amplified using the same method but different primers from the scAAV9-cytomegalovirus (CMV)-GFP vector plasmid, previously described in Tanguy et al.[49] PCR fragments were cloned in the recombinant plasmid (pscAAV9)-PGK-survival of motor neuron gene (SMN) described in Besse et al.,[43] following digestion with Hind III and Not I (unique restriction sites) to eliminate the chimeric intron and the cDNA. Ligation with PCR-amplified GLA cDNA was performed with Quick Ligation (NEB; #M2200S). The ligated vector was transformed in XL10-Gold ultracompetent cells (Agilent Technologies), and DNA was extracted to identify positive colonies by enzymatic restriction. Correctly oriented clones were selected by sequencing with primers aligned to the vector.

Virus Production

The viral particles were produced following the protocol described in Biferi et al.[23] Briefly, HEK293T cells were cotransfected, using polyethylenimine, with the adenovirus helper plasmid (pXX6Helper), the rep2 cap9-encoding plasmid (AAV9 capsid), and either pscAAV9-PGK-GLA or pscAAV9-PGK-GFP plasmids. Following 72 h

incubation at 37°C, cells were harvested, and viral particles were purified through an iodixanol gradient. Virus titer, expressed as vg per milliliter, was measured by qPCR using specific primers and virus standard curve with known concentrations.

Animals, Injections, and Tissue Harvesting

Wild-type FVB/NRj mice (Janvier Labs) were used to perform a pilot study to assess vector activity. Animals were maintained in the Centre of Functional Evaluation-UMS28 (Sorbonne University, Paris, France) under controlled conditions (22 ± 2°C, 50 ± 10% relative humidity, 12 h/12 h light/dark cycle, food and water *ad libitum*). All animal procedures followed the European guidelines for the care and use of experimental animals.

B6;129-Gla^{tm1Kul}*/J* (FD mice; The Jackson Laboratory; #3535) were maintained in the animal facility at Vigo University (Servicio de Bioexperimentación SB-UVi REGA; ES360570215601), in accordance with external and internal biosafety and bioethics guidelines. The experimental procedures (ES360570215601/17/INVMED02/OUTROS04/SO01 and SO02) were approved by Vigo University Committee (0001-2017SO and 00003-2017SO) and authorized by the competent authority (Xunta de Galicia, Conselleria do Medio Rural, Pontevedra, Spain).

Mice were identified at P1 with ink tattoos in the fingers and genotyped following the protocol indicated by The Jackson Laboratory for this strain.

For the first therapeutic test in newborn FD mice, groups of 4 hemizygous newborn mice, between P1 and P3, were injected with either scAAV9-PGK-GLA or scAAV9-PGK-GFP through the temporal vein (40 µL of viral solution at 1.3×10^{13} vg/mL). These treated animals and a control group of noninjected hemizygous or wild-type animals were maintained in the experiment for either 3 or 5 months. At the end points, organs (brain, spinal cord, heart, liver, kidney, and spleen) were removed and divided in two tubes: one snap frozen in liquid nitrogen for biochemical assays and one containing paraformaldehyde (PFA; 4% v/v). In subgroups of mice, tissue fragments were embedded in glutaraldehyde for ultrastructural analysis.

In adult FD mice, the scAAV9-PGK-GLA was injected in groups of 4 hemizygous and heterozygous animals at 1 month or 3 months of age to assess presymptomatic and symptomatic treatment, respectively. Viral suspension (3.13×10^{13} vg/mL) was injected in the tail vein at two different doses (6×10^{13} vg/kg or 1.8×10^{14} vg/kg) in each group of animals; volume of vector solution was adjusted to compensate for weight differences.

As control groups, noninjected wild-type or knockout mice of both sexes were used. Total number of animals N = 64, as described in Table 2. Submandibular vein blood withdrawal was performed at baseline (before injection), at 4 months following injection, and at the end of the protocol. 5 months after the administration of the vector, as described for newborn mice, animals were sacrificed by lethal injection (200 mg/kg ketamine and 30 mg/kg xylazine) to collect brain, spinal cord, heart, liver, kidney, spleen, thymus, and skeletal muscle. An oriented fragment of the organs was fixed in PFA and used for immunohistochemistry. The remaining tissues were snap frozen and then lysed for biochemical assessments. Brains were divided in hemispheres; one was embedded in PFA, and the other was consistently cut, as evenly as possible, in three fragments that were used for the biochemical analyses with the appropriate lysing protocol.

AAV9 Particle Distribution in Tissues

DNA was automatically extracted from frozen tissue sections on the QIAcube platform, using the DNeasy kit (#69504; QIAGEN) and QIAamp Mini Rotor Adaptor (#1064532; QIAGEN). Absolute quantification was determined by ddPCR testing DNA samples (2.5 ng/µL) in duplicates. Primers/probe mix was specific for the recombinant AAV9 genome (primers: 5′-TCCATCACTAGGG GTTCCTTG-3′ and 5′-GTAGATAAGTAGCATGGC-3′, 900 nM; probe: Fluorescein-AMester-5′-TAGTTAATGATTAACCC-3′-Quencher, 250 nM). Negative (no template control [NTC]) and positive (scAAV9-PGK-GLA particles 10^3 vg/µL) controls were used in each experiment. Droplets were automatically generated with a QX200 Automated Droplet Generator (Bio-Rad). ddPCR was performed using the following cycling conditions: 10 min at 95°C, 40 cycles of two-step thermal profile: 95°C at 30 s and 57.5°C at 60 s with a ramp rate of 2°C/s. Plates were finally transferred to a QX200 Droplet Reader (Bio-Rad), and data analysis was performed using QuantaSoft software (Bio-Rad). The threshold separating negative and positive droplets was set manually just above the cluster of negative droplets. Data from wells with number of droplets below 10,000 were excluded from analysis. Results were expressed as vg/dg (vector copies per ng of extracted DNA).

Expression of Human α-GalA in Tissue Lysates

Relative expression levels of α-GalA in tissues were determined by WB. Briefly, tissues were lysed with lysis buffer (#B9803; Cell Signaling Technology) containing protease inhibitor cocktail (#P8340; Sigma-Aldrich), homogenized with Ultra-Turrax, sonicated, and centrifuged 20 min at 10,000 × *g* (4°C) to collect cytosolic fractions. Proteins were separated through SDS-PAGE in 4%–15% polyacrylamide stain-free Mini-Protean or Criterion TGX gels (#4568083, #5678081; Bio-Rad) and transferred to 0.2 µm polyvinylidene fluoride (PVDF) membranes (Transblot Turbo, #1704157; Bio-Rad). The membranes were blotted with a monoclonal anti-human-α-GalA antibody (#ab129173; Abcam). Total load was estimated using Image Lab software (Bio-Rad), by imaging the activated stain-free gels and following the recommendations of the manufacturer. Each antigen band was normalized to its total protein lane (Figure S8) using the total protein normalization tool (Image Lab Software) and following the manufacturer's protocol. Band intensity values were divided for the intensity value obtained in noninjected hemizygous or heterozygous control sample (background).

α-GalA Enzymatic Activity Assay

Activity of α-GalA was measured using the method of Chamoles et al.[50] Briefly, tissues were embedded in deionized water (300 μL) and subjected to three freeze-thaw cycles before homogenization with the Ultra-Turrax homogenizer (IKA-Werke). The preparations were sonicated and centrifuged at 10,000 × *g* to collect cytosolic fractions. The activity of cell lysates was measured in 0.15 M phosphate-citrate buffer (pH 4.2) in the presence of the substrate, 4 mM 4-methylumbelliferyl-α-D-galactopyranoside (Glycosynth) and 50 mM N-acetyl-D-galactosamine (#A2795; Sigma-Aldrich). The reactions were incubated for 2 h at 37°C, and at this point, the stopping solution (0.1 M ethylenediamine, pH 11.4) was added to halt the reaction. Then, the fluorescence from samples was read using a Twinkle LB 970 fluorometer (Berthold) at 360 nm excitation and 450 nm emission wavelengths. Specific activity was expressed as nanomoles of hydrolyzed substrate per hour and milligram of total protein, extrapolating nanomoles of hydrolyzed substrate from a standard curve (fluorescence versus known concentrations of 4-methylumbelliferone; Merck; #M1381). Total protein concentration was measured with the Pierce Bicinchoninic Acid (BCA) Protein Assay Kit (Thermo Fisher Scientific), following the manufacturer's protocol.

Gb3 and Lyso-Gb3 Deposits Quantification and Distribution

Lyso-Gb3 was quantified by LC-MS in tissue and plasma samples using the protocol described by Nowak et al.[51] This analysis was performed at ARCHIMED Life Science (Vienna, Austria). Plasma samples were collected at pre-dose at 4 months and at 5 months following injection. Tissue lysates were prepared as described for enzymatic activity measurements, and lipid extraction was performed at ARCHIMED Life Science. Lyso-Gb3 concentration in tissue was expressed as nanograms per milligrams of protein and in plasma as nanograms per milliliter of sample.

Distribution of affected lysosomes was examined by Gb3 immunostaining with anti-CD77 antibody (clone BGR23; #A2506; AMS Biotechnology) and costaining with 4′,6-diamidino-2-phenylindole (DAPI) and/or rhodamine phalloidin to detect nuclei and membranes (polymerized actin), respectively. Immunohistochemistry was performed on frozen tissues sections of 10 μm. For spinal cord samples, organs were decalcified overnight before organs were decalcified overnight (acetic acid 10% v/v in saline solution containing PFA 4% v/v) before freezing and cutting tissue. Fixed preparations were permeabilized (phosphate-buffered saline [PBS], bovine serum albumin [BSA] 5%, Triton 0.01%) and treated with 0.01 M citrate phosphate buffer (pH 6; 5′ at 85°C) for antigenic retrieval. Images were taken with a conventional fluorescence microscope DM6 equipped with a DFC550 camera (Leica; Figures 2, 7A, S5, and S10) or the inverted microscope DMi6000B with a DFC365FX camera (Leica; Figures 7B and S12). Quantitative assessment of deposits was performed using the quantification tool of LAS AF software (Leica) and expressed as mean fluoresce intensity (pixel gray levels).

Ultrastructural analysis was performed by transmission-electron microscopy in selected samples. Rectangular pieces for electron microscopy were fixed in 2.5% glutaraldehyde, post-fixed in osmium tetroxide, and embedded in Epon after routine dehydration. Semi-thin sections were stained with toluidine blue, and ultra-thin sections were contrasted with uranyl acetate and lead citrate and mounted in copper grids. Ultra-thin sections were examined with a Philips CM100 transmission electron microscope.

Antibody Production against Human α-GalA

To assess the immunoresponse of α-GalA, an ELISA test in plasma samples was set up to detect anti-human α-GalA IgG antibodies. Briefly, clear 96-well plates (Nunc-Immuno MicroWell 96-well solid plate;, Merck) were coated with 1 μg/mL α-GalA (#6164-GH; R&D Systems) and incubated overnight at 4°C. Plates were blocked with 2% BSA in PBS at 4°C. Serum samples were diluted (1:100 in blocking solution) and incubated for 90 min at 37°C. Antibodies binding α-GalA were detected using horseradish peroxidase (HRP)-conjugated goat anti-mouse IgG antibodies (1:10,000) (# ab6789; Abcam). Samples were incubated 1 h at room temperature and then visualized using the BioFX TMB/Stop solution (#ab171522; Abcam). The reaction was halted with 1 vol of HCl 0.1 N. Absorbance was measured at 450 nm. IgG concentrations were calculated referring to a standard curve of commercial anti-human GLA antibody (#ab129173; Abcam) and donkey anti-rabbit IgG polyclonal secondary antibodies (#NA934; GE Healthcare).

Statistical Analysis

Power analysis to determine the number of animals to be included in each group was performed with the software InVivoStat, assuming that α-GalA activity would increase at least 2 nmol/h × mg in hemizygous animals injected with the scAAV9-PGK-GLA vector (power 80% and $p > 0.05$). For ddPCR, WB, activity, and Lyso-Gb3 data, significance was assessed by nonparametric t tests (2 tales) using Graph Prism software.

For each tissue, time point, and doses, the correlation among variables (virus titer, α-GalA expression, and activity) was assessed using Rho.

Statistical differences in the body weight were assessed by mixed ANOVA, combining Mauchly's test of sphericity and Greenhouse-Geisser correction.

SUPPLEMENTAL INFORMATION

Supplemental Information can be found online at https://doi.org/10.1016/j.omtm.2020.10.016.

ACKNOWLEDGMENTS

We acknowledge Archimed Life Science, Vienna, Austria, for LC-MS detection of Lyso-Gb3 and Marina Peña Penabad at the Animal Facility Servicio de Bioexperimentación of Vigo University (SB-UVi, REGA; ES360570215601). We also acknowledge Cristina Martínez Reglero from the Methodology and Statistic Unit of IIS-Galicia Sur for the support with statistical analysis. The web page Biorender.com was used to design the graphical abstract. This project was sponsored by the French patients' association Vaincre Les Maladies

Lysosomales (AO2017-3 to S.O.), cofunded by AFM-Téléthon, France; the Instituto de Salud Carlos III, Spain, through the projects PI11/00842 and PI19/01886, cofunded by European Regional Development Fund "A Way to Make Europe" (to S.O.); and BIOCAPS Project (FP7REGPOT216325; European Union; to A.G.-F.). M.G.B., M.C.-T., and T.M. were sponsored by the Association Institut de Myologie (AIM) in the Centre of Research in Myology, Sorbonne Université, and the Institut National de la Santé et de la Recherche Médicale (Paris, France). A contract for A.G.-S. was supported by the Spanish government through the action PEJ2018-005289-A (Aid for the Promotion of Youth Employment and Implementation of the Youth Guarantee in R+D+i 2018, Ministerio de Ciencia e Innovación), cofunded by the European Social Fund "Investing in Your Future."

AUTHOR CONTRIBUTIONS

M.G.B. designed the vectors and participated in the analysis of the results and in the writing of the manuscript. M.C.-T. prepared the viral particles for injections. A.G.-S. and S.T.-B. performed western blot analysis of α-GalA in the different tissues and enzymatic activity assays. A.G.-S. also prepared the figures of the paper and analyzed the data. O.S.-R., B.S.-M.-T., and S.B. performed immunohistochemistry and ultrastructural analysis of tissues and the interpretation of the results. I.V.-G. and T.P.M. performed DNA isolation from tissues and the determination of viral titration and distribution in tissues. T.M., A.F.-C., and V.D. took care of animal maintenance, monitoring, and dosing. A.G.-F. helped to design the animal experimental project and develop the serum antibody detection assay. She also revised the manuscript. M.B. supervised the study. S.O. designed the project, participated in vector development and in all of the experiments, analyzed the data, and wrote the manuscript.

DECLARATION OF INTERESTS

The authors declare no competing interests.

REFERENCES

1. Elliott, S., Buroker, N., Cournoyer, J.J., Potier, A.M., Trometer, J.D., Elbin, C., Schermer, M.J., Kantola, J., Boyce, A., Turecek, F., et al. (2016). Pilot study of newborn screening for six lysosomal storage diseases using Tandem Mass Spectrometry. Mol. Genet. Metab. *118*, 304–309.
2. Hopkins, P.V., Campbell, C., Klug, T., Rogers, S., Raburn-Miller, J., and Kiesling, J. (2015). Lysosomal storage disorder screening implementation: findings from the first six months of full population pilot testing in Missouri. J. Pediatr. *166*, 172–177.
3. Mehta, A. (2010). Clinical manifestations of Fabry disease: an overview. In Fabry Disease, D. Elstein, G. Altarescu, and M. Beck, eds. (Springer), pp. 181–187.
4. Dobrovolny, R., Dvorakova, L., Ledvinova, J., Magage, S., Bultas, J., Lubanda, J.C., Elleder, M., Karetova, D., Pavlikova, M., and Hrebicek, M. (2005). Relationship between X-inactivation and clinical involvement in Fabry heterozygotes. Eleven novel mutations in the α-galactosidase A gene in the Czech and Slovak population. J. Mol. Med. (Berl.) *83*, 647–654.
5. Oder, D., Nordbeck, P., and Wanner, C. (2016). Long Term Treatment with Enzyme Replacement Therapy in Patients with Fabry Disease. Nephron *134*, 30–36.
6. Germain, D.P., Hughes, D.A., Nicholls, K., Bichet, D.G., Giugliani, R., Wilcox, W.R., Feliciani, C., Shankar, S.P., Ezgu, F., Amartino, H., et al. (2016). Treatment of Fabry's Disease with the Pharmacologic Chaperone Migalastat. N. Engl. J. Med. *375*, 545–555.
7. Biffi, A. (2016). Gene therapy for lysosomal storage disorders: a good start. Hum. Mol. Genet. *25* (R1), R65–R75.
8. Ortolano, S. (2016). Small molecules: Substrate inhibitors, chaperones, stop-codon read through, and beyond. JIEMS *4*, 1–11.
9. Leinekugel, P., Michel, S., Conzelmann, E., and Sandhoff, K. (1992). Quantitative correlation between the residual activity of β-hexosaminidase A and arylsulfatase A and the severity of the resulting lysosomal storage disease. Hum. Genet. *88*, 513–523.
10. Ries, M., Clarke, J.T.R., Whybra, C., Timmons, M., Robinson, C., Schlaggar, B.L., Pastores, G., Lien, Y.H., Kampmann, C., Brady, R.O., et al. (2006). Enzyme-replacement therapy with agalsidase alfa in children with Fabry disease. Pediatrics *118*, 924–932.
11. Ortolano, S., Spuch, C., and Navarro, C. (2012). Present and future of adeno associated virus based gene therapy approaches. Recent Pat. Endocr. Metab. Immune Drug Discov. *6*, 47–66.
12. Colella, P., Ronzitti, G., and Mingozzi, F. (2017). Emerging Issues in AAV-Mediated *In Vivo* Gene Therapy. Mol. Ther. Methods Clin. Dev. *8*, 87–104.
13. Ogawa, K., Hirai, Y., Ishizaki, M., Takahashi, H., Hanawa, H., Fukunaga, Y., and Shimada, T. (2009). Long-term inhibition of glycosphingolipid accumulation in Fabry model mice by a single systemic injection of AAV1 vector in the neonatal period. Mol. Genet. Metab. *96*, 91–96.
14. Ziegler, R.J., Lonning, S.M., Armentano, D., Li, C., Souza, D.W., Cherry, M., Ford, C., Barbon, C.M., Desnick, R.J., Gao, G., et al. (2004). AAV2 vector harboring a liver-restricted promoter facilitates sustained expression of therapeutic levels of α-galactosidase A and the induction of immune tolerance in Fabry mice. Mol. Ther. *9*, 231–240.
15. Ziegler, R.J., Cherry, M., Barbon, C.M., Li, C., Bercury, S.D., Armentano, D., Desnick, R.J., and Cheng, S.H. (2007). Correction of the biochemical and functional deficits in Fabry mice following AAV8-mediated hepatic expression of α-galactosidase A. Mol. Ther. *15*, 492–500.
16. Sharma, R., Anguela, X.M., Doyon, Y., Wechsler, T., DeKelver, R.C., Sproul, S., Paschon, D.E., Miller, J.C., Davidson, R.J., Shivak, D., et al. (2015). In vivo genome editing of the albumin locus as a platform for protein replacement therapy. Blood *126*, 1777–1784.
17. Huang, J., Khan, A., Au, B.C., Barber, D.L., López-Vásquez, L., Prokopishyn, N.L., Boutin, M., Rothe, M., Rip, J.W., Abaoui, M., et al. (2017). Lentivector Iterations and Pre-Clinical Scale-Up/Toxicity Testing: Targeting Mobilized $CD34^+$ Cells for Correction of Fabry Disease. Mol. Ther. Methods Clin. Dev. *5*, 241–258.
18. Altarescu, G., Moore, D.F., and Schiffmann, R. (2005). Effect of genetic modifiers on cerebral lesions in Fabry disease. Neurology *64*, 2148–2150.
19. Shi, Q., Chen, J., Pongmoragot, J., Lanthier, S., and Saposnik, G. (2014). Prevalence of Fabry disease in stroke patients–a systematic review and meta-analysis. J. Stroke Cerebrovasc. Dis. *23*, 985–992.
20. Sims, K., Politei, J., Banikazemi, M., and Lee, P. (2009). Stroke in Fabry disease frequently occurs before diagnosis and in the absence of other clinical events: natural history data from the Fabry Registry. Stroke *40*, 788–794.
21. Foust, K.D., Nurre, E., Montgomery, C.L., Hernandez, A., Chan, C.M., and Kaspar, B.K. (2009). Intravascular AAV9 preferentially targets neonatal neurons and adult astrocytes. Nat. Biotechnol. *27*, 59–65.
22. Duque, S., Joussemet, B., Riviere, C., Marais, T., Dubreil, L., Douar, A.M., Fyfe, J., Moullier, P., Colle, M.A., and Barkats, M. (2009). Intravenous administration of self-complementary AAV9 enables transgene delivery to adult motor neurons. Mol. Ther. *17*, 1187–1196.
23. Biferi, M.G., Cohen-Tannoudji, M., Cappelletto, A., Giroux, B., Roda, M., Astord, S., Marais, T., Bos, C., Voit, T., Ferry, A., and Barkats, M. (2017). A New AAV10-U7-Mediated Gene Therapy Prolongs Survival and Restores Function in an ALS Mouse Model. Mol. Ther. *25*, 2038–2052.
24. Ohshima, T., Murray, G.J., Swaim, W.D., Longenecker, G., Quirk, J.M., Cardarelli, C.O., Sugimoto, Y., Pastan, I., Gottesman, M.M., Brady, R.O., and Kulkarni, A.B. (1997). α-Galactosidase A deficient mice: a model of Fabry disease. Proc. Natl. Acad. Sci. USA *94*, 2540–2544.
25. Bangari, D.S., Ashe, K.M., Desnick, R.J., Maloney, C., Lydon, J., Piepenhagen, P., Budman, E., Leonard, J.P., Cheng, S.H., Marshall, J., and Thurberg, B.L. (2015).

α-Galactosidase A knockout mice: progressive organ pathology resembles the type 2 later-onset phenotype of Fabry disease. Am. J. Pathol. *185*, 651–665.

26. Mendell, J.R., Al-Zaidy, S., Shell, R., Arnold, W.D., Rodino-Klapac, L.R., Prior, T.W., Lowes, L., Alfano, L., Berry, K., Church, K., et al. (2017). Single-dose gene-replacement therapy for spinal muscular atrophy. N. Engl. J. Med. *377*, 1713–1722.

27. Hoy, S.M. (2019). Onasemnogene Abeparvovec: First Global Approval. Drugs *79*, 1255–1262.

28. Obata, F., and Obrig, T. (2010). Distribution of Gb(3) Immunoreactivity in the Mouse Central Nervous System. Toxins (Basel) *2*, 1997–2006.

29. Rodrigues, L.G., Ferraz, M.J., Rodrigues, D., Pais-Vieira, M., Lima, D., Brady, R.O., Sousa, M.M., and Sá-Miranda, M.C. (2009). Neurophysiological, behavioral and morphological abnormalities in the Fabry knockout mice. Neurobiol. Dis. *33*, 48–56.

30. Hofmann, L., Hose, D., Grießhammer, A., Blum, R., Döring, F., Dib-Hajj, S., Waxman, S., Sommer, C., Wischmeyer, E., and Üçeyler, N. (2018). Characterization of small fiber pathology in a mouse model of Fabry disease. eLife *7*, e39300.

31. Hofmann, L., Karl, F., Sommer, C., and Üçeyler, N. (2017). Affective and cognitive behavior in the alpha-galactosidase A deficient mouse model of Fabry disease. PLoS ONE *12*, e0180601.

32. Sakuraba, H., Togawa, T., Tsukimura, T., and Kato, H. (2018). Plasma lyso-Gb3: a biomarker for monitoring fabry patients during enzyme replacement therapy. Clin. Exp. Nephrol. *22*, 843–849.

33. Desnick, R.J. (2020). Fabry disease: α-galactosidase A deficiency. In Rosenberg's Molecular and Genetic Basis of Neurological and Psychiatric Disease, Roger N. Rosenberg and Juan M. Pascual, eds. (Academic Press), pp. 575–587.

34. Tabira, T., Goto, I., Kuroiwa, Y., and Kikuchi, M. (1974). Neuropathological and biochemical studies in Fabry's disease. Acta Neuropathol. *30*, 345–354.

35. Wise, A.H., Yang, A., Naik, H., Stauffer, C., Zeid, N., Liong, C., Balwani, M., Desnick, R.J., and Alcalay, R.N. (2017). Parkinson's disease prevalence in Fabry disease: A survey study. Mol. Genet. Metab. Rep. *14*, 27–30.

36. Nietupski, J.B., Hurlbut, G.D., Ziegler, R.J., Chu, Q., Hodges, B.L., Ashe, K.M., Bree, M., Cheng, S.H., Gregory, R.J., Marshall, J., and Scheule, R.K. (2011). Systemic administration of AAV8-α-galactosidase A induces humoral tolerance in nonhuman primates despite low hepatic expression. Mol. Ther. *19*, 1999–2011.

37. Yasuda, M., Shabbeer, J., Osawa, M., and Desnick, R.J. (2003). Fabry disease: novel α-galactosidase A 3′-terminal mutations result in multiple transcripts due to aberrant 3′-end formation. Am. J. Hum. Genet. *73*, 162–173.

38. Hordeaux, J., Hinderer, C., Buza, E.L., Louboutin, J.P., Jahan, T., Bell, P., Chichester, J.A., Tarantal, A.F., and Wilson, J.M. (2019). Safe and Sustained Expression of Human Iduronidase After Intrathecal Administration of Adeno-Associated Virus Serotype 9 in Infant Rhesus Monkeys. Hum. Gene Ther. *30*, 957–966.

39. Laoharawee, K., Podetz-Pedersen, K.M., Nguyen, T.T., Evenstar, L.B., Kitto, K.F., Nan, Z., Fairbanks, C.A., Low, W.C., Kozarsky, K.F., and McIvor, R.S. (2017). Prevention of neurocognitive deficiency in mucopolysaccharidosis Type II mice by central nervous system-directed, AAV9-mediated iduronate sulfatase gene transfer. Hum. Gene Ther. *28*, 626–638.

40. Belur, L.R., Temme, A., Podetz-Pedersen, K.M., Riedl, M., Vulchanova, L., Robinson, N., Hanson, L.R., Kozarsky, K.F., Orchard, P.J., Frey, W.H., 2nd, et al. (2017). Intranasal Adeno-Associated Virus Mediated Gene Delivery and Expression of Human Iduronidase in the Central Nervous System: A Noninvasive and Effective Approach for Prevention of Neurologic Disease in Mucopolysaccharidosis Type I. Hum. Gene Ther. *28*, 576–587.

41. Hughes, D., Mikosch, P., Belmatoug, N., Carubbi, F., Cox, T., Goker-Alpan, O., Kindmark, A., Mistry, P., Poll, L., Weinreb, N., and Deegan, P. (2019). Gaucher Disease in Bone: From Pathophysiology to Practice. J. Bone Miner. Res. *34*, 996–1013.

42. Link, B., Lapagesse de Camargo Pinto, L., Giugliani, R., Wraith, J.E., Guffon, N., Eich, E., and Beck, M. (2010). Orthopedic challenges in patients with mucopolysaccharidoses type II (Hunter syndrome) enrolled in the Hunter Outcome Survey (HOS). Orthop. Rev. *2*, e16.

43. Besse, A., Astord, S., Marais, T., Roda, M., Giroux, B., Lejeune, F.X., Relaix, F., Smeriglio, P., Barkats, M., and Biferi, M.G. (2020). AAV9-Mediated Expression of SMN Restricted to Neurons Does Not Rescue the Spinal Muscular Atrophy Phenotype in Mice. Mol. Ther. *28*, 1887–1901.

44. Novartis (2020). Zolgensma® data shows rapid, significant, clinically meaningful benefit in SMA including prolonged event free survival, motor milestone achievement and durability now up to 5 years post-dosing, https://www.avexis.com/Content/pdf/newsarticle-IVasset-20200323.pdf.

45. Spear, P.G., and Edelman, G.M. (1974). Maturation of the humoral immune response in mice. J. Exp. Med. *139*, 249–263.

46. Vono, M., Eberhardt, C.S., Auderset, F., Mastelic-Gavillet, B., Lemeille, S., Christensen, D., Andersen, P., Lambert, P.H., and Siegrist, C.A. (2019). Maternal Antibodies Inhibit Neonatal and Infant Responses to Vaccination by Shaping the Early-Life B Cell Repertoire within Germinal Centers. Cell Rep. *28*, 1773–1784.e5.

47. Audentes Therapeutics (2020). Letter to the XLMTM Patient Community, https://myotubulartrust.org/wp-content/uploads/23JUNE2020-Letter-to-Patient-Community_Sent.pdf.

48. Ruiz de Garibay, A.P., Delgado, D., Del Pozo-Rodríguez, A., Solinís, M.Á., and Gascón, A.R. (2012). Multicomponent nanoparticles as nonviral vectors for the treatment of Fabry disease by gene therapy. Drug Des. Devel. Ther. *6*, 303–310.

49. Tanguy, Y., Biferi, M.G., Besse, A., Astord, S., Cohen-Tannoudji, M., Marais, T., and Barkats, M. (2015). Systemic AAVrh10 provides higher transgene expression than AAV9 in the brain and the spinal cord of neonatal mice. Front. Mol. Neurosci. *8*, 36.

50. Chamoles, N.A., Blanco, M., and Gaggioli, D. (2001). Fabry disease: enzymatic diagnosis in dried blood spots on filter paper. Clin. Chim. Acta *308*, 195–196.

51. Nowak, A., Mechtler, T.P., Desnick, R.J., and Kasper, D.C. (2017). Plasma LysoGb3: A useful biomarker for the diagnosis and treatment of Fabry disease heterozygotes. Mol. Genet. Metab. *120*, 57–61.

OMTM, Volume *20*

Supplemental Information

Systemic Treatment of Fabry Disease Using a Novel AAV9 Vector Expressing α-Galactosidase A

Maria Grazia Biferi, Mathilde Cohen-Tannoudji, Andrea García-Silva, Olga Souto-Rodríguez, Irene Viéitez-González, Beatriz San-Millán-Tejado, Andrea Fernández-Carrera, Tania Pérez-Márquez, Susana Teijeira-Bautista, Soraya Barrera, Vanesa Domínguez, Thibaut Marais, África González-Fernández, Martine Barkats, and Saida Ortolano

Figure S1 The scAAV9-PGK-GLA drives widespread expression of functional α-GalA when it is injected *in vivo.*

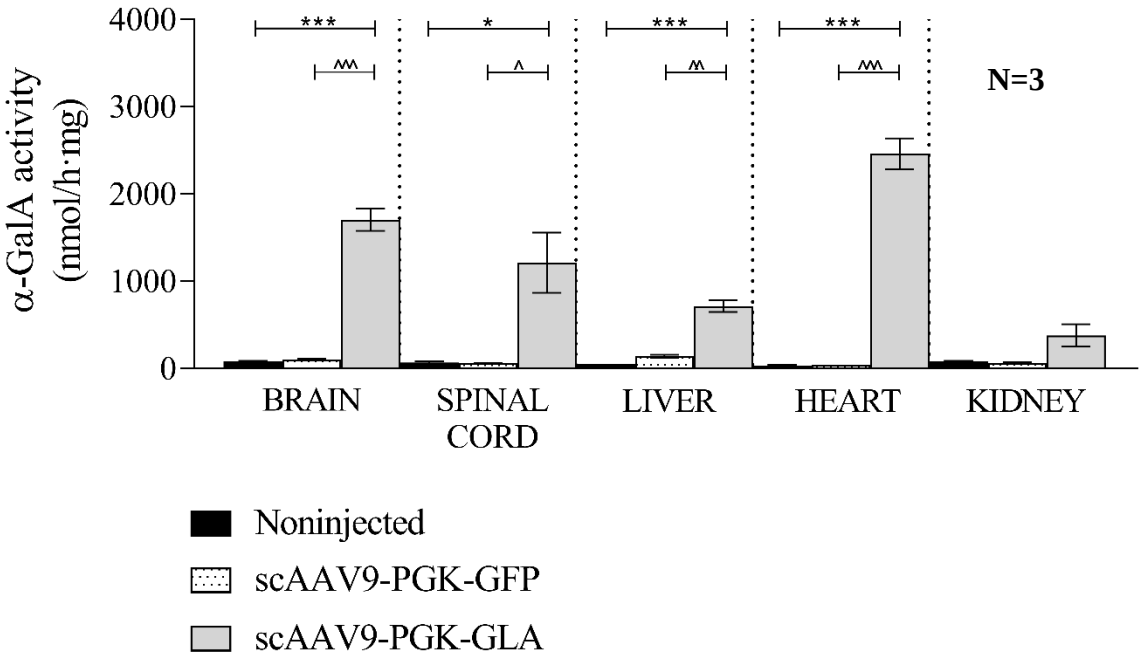

Activity of α-GalA was measured in tissues (brain, spinal cord, liver, heart and kidney) from FVB/NRj newborn mice injected (i.v. and i.c.v. at $3.2 \cdot 10^{14}$ vg/kg) with either scAAV9-PGK-GLA or scAAV9-PGK-GFP vectors, two months after treatment. Three animals per group were treated, N=3. Values (mean ± SEM) were compared with those obtained in the same tissues of age-matched noninjected mice of the same strain. Statistical analysis was assessed by nonparamentric t-test between animals treated with scAAV9-PGK-GLA and non-injected animals (* $p<0.05$; ** $p<0.01$;*** $p<0.001$) or between the two treatments (^ $p<0.05$; ^^ $p<0.01$;^^^ $p<0.001$).

The combined i.v. and i.c.v. injection of scAA9-PGK-GLA drives high levels of functional α-GalA expression in the analyzed tissues, including the CNS.

Figure S2 scAAV9-PGK-GLA prevents the formation of intralysosomal electron-dense inclusions in cardiac interstitial fibroblasts, cardiomyocytes and endothelial cells from a 3 months old FD hemizygous mouse treated at birth.

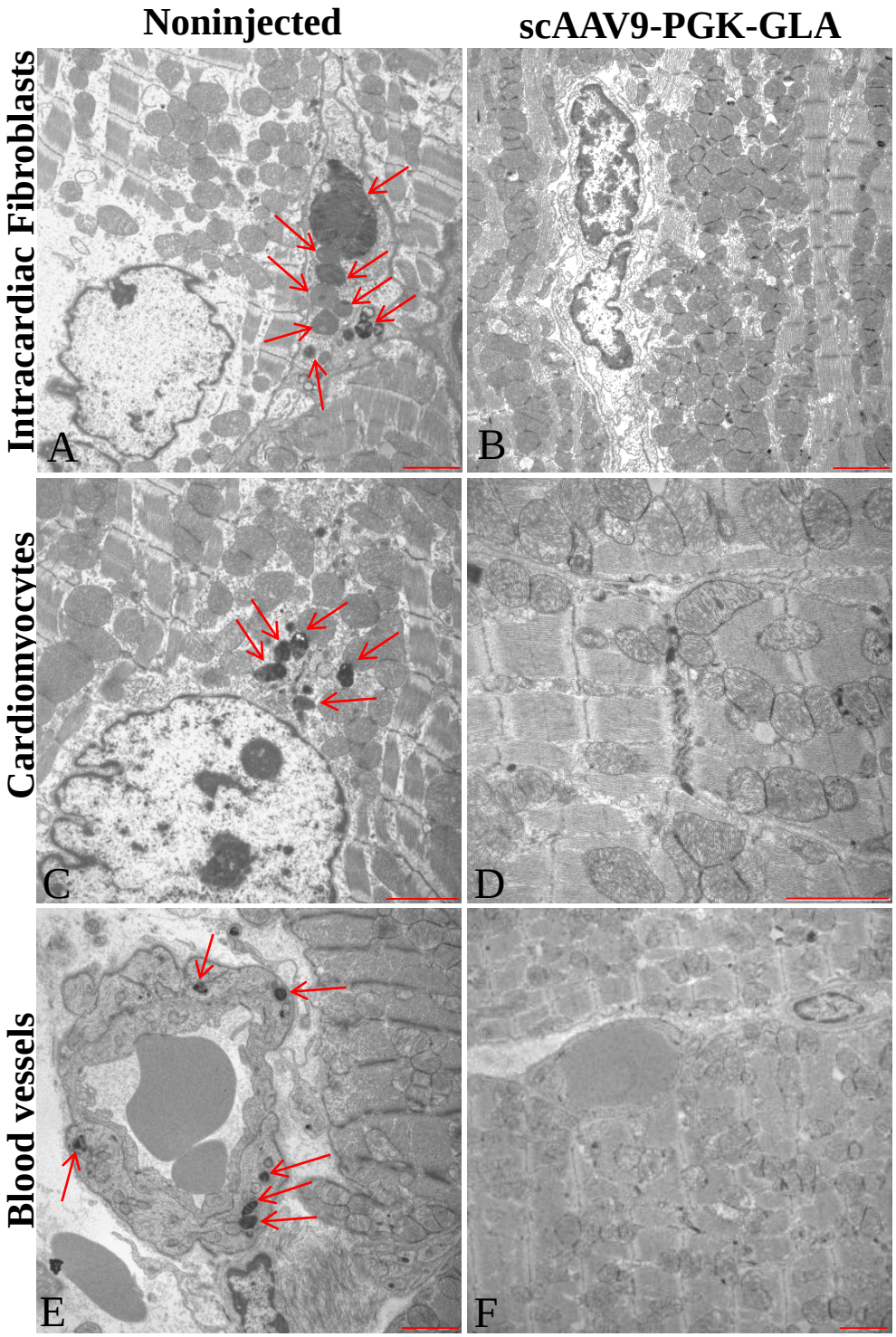

Transmission-electron microscopy of ultrathin myocardial tissue sections from hemizygous newborn FD mice injected or not with scAAV9-PGK-GLA (i.v.) and sacrificed 3 months following injection. Panel A-C-E show how interstitial fibroblasts, cardiomyocytes and vessel endothelial cells in the heart from a noninjected mouse present abundant intralysosomal electron-dense inclusions and multilamellar electrondense bodies (zebra bodies). In contrast, these cells are free of deposits in a mouse treated with scAAV9-PGK-GLA (Panels B-D-F). Scale bar= 2µm. Red arrows appoint to intralysosomal inclusions.

Figure S3 Ultrastructural analysis reveals that scAAV9-PGK-GLA reduces the formation of intralysosomal inclusions in epithelial tubular cells of kidneys from a hemizygous FD newborn mouse injected with the vector at birth.

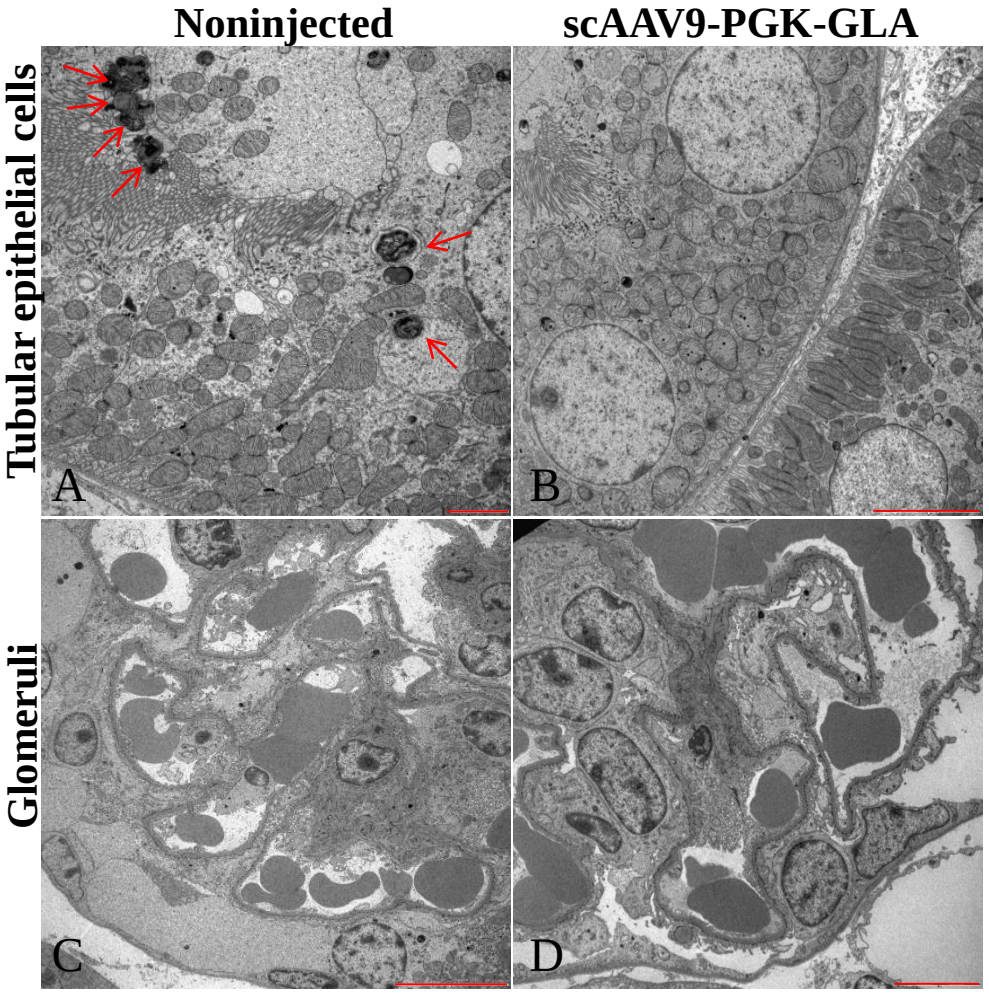

Transmission-electron microscopy of ultrathin kidney slices from a hemizygous newborn FD mouse sacrificed 3 months following injection with scAAV9-PGK-GLA (i.v. between P1 and P3) and a non-injected control.
Noninjected hemizygous mouse (A) shows intralysosomal electron-dense inclusions in the cytosol of epithelial tubular cells of the kidney, while these inclusions are less frequent in the same cells from a mouse injected with scAAV9-PGK-GLA. (B) shows tubular epithelial cells without intralysosomal inclusions from a treated mouse. In kidneys from either noninjected (C) or treated mice (D) no inclusions were observed in the cells of the glomeruli. Scale bar=2µm in (A); 5µm (B-D); and 10µm in (C). Red arrows appoint to intralysosomal inclusions.

Figure S4 Intralysosomal electron-dense inclusions typical of FD cannot be detected in hepatocytes, and CNS cells from a 3 months old FD hemizygous mouse.

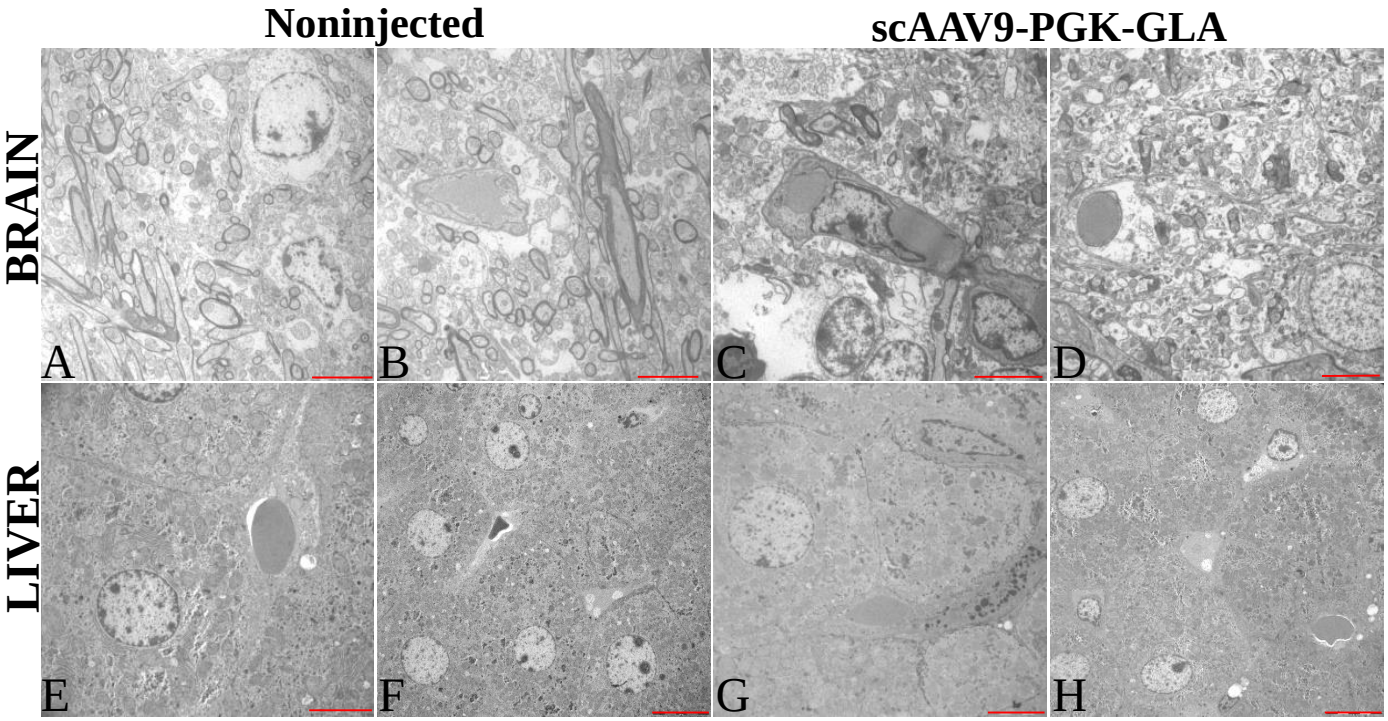

Transmission-electron microscopy of ultrathin brain and and slices from a hemizygous newborn FD mouse sacrificed 3 months following injection with scAAV9-PGK-GLA (i.v.) and a noninjected control. Panels A-D show cells (neuron and glial cells) of the brain from a noninjected mouse (A-B) and from an animal injected with scAAV9-PGK-GLA (C-D).

Panels E-H show hepatocytes from a non-injected FD mouse (E-F) and from an animal injected with scAAV9-PGK-GLA (Panel G-H). Scale bar=5µm in A, B, C, D, E and G, while Scale bar=10µm in F and H.

Electron-dense intralysosomal inclusions cannot be detected in hepatocytes, cerebral neurons and glial cells from either injected or noninjected animals.

Figure S5 Gb3 is expressed in the cerebellum of FD mice independently of the genotype and it is reduced after treatment with scAVV9-PGK-GLA

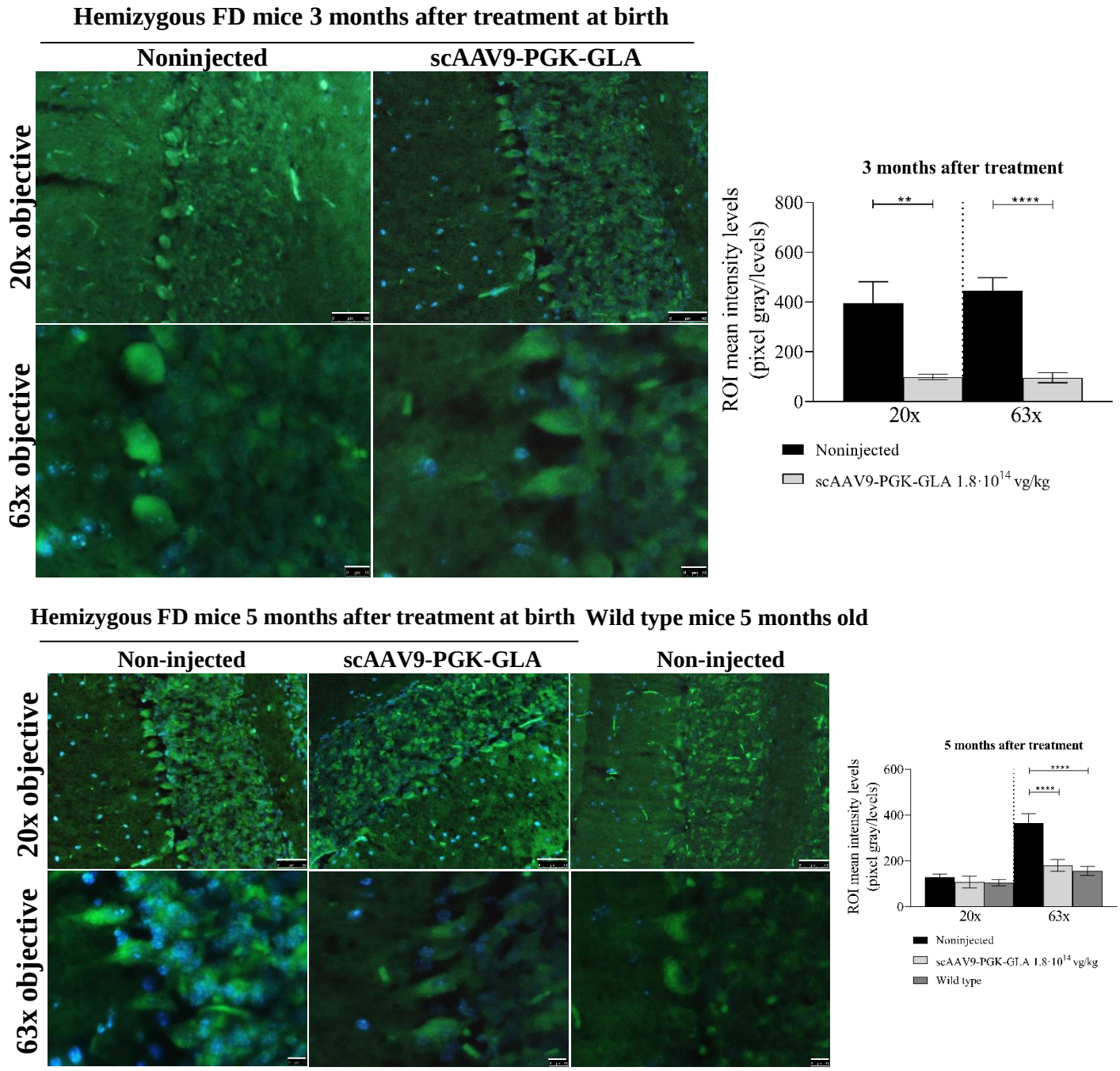

Representative immunofluorescence images of cerebellum from FD mice 3 or 5 months after treatment with scAAV9-PGK-GLA and noninjected hemizygous or wild type controls. Gb3 signal was detected with an anti-Gb3 antibody (green) and nuclei were stained with DAPI. Scale bar=50µm for 20X objective images and scale bar=10µm for 63X objective pictures. Histograms represent mean fluorescence in green channel (mean pixel intensity) as computed in different regions of interest (ROI) with constant area defined for each image. Error is expressed as SEM. Significance of the data, comparing each value with the value of the corresponding noninjected control was assessed by nonparametric t-test (*p<0.05; **p<0.01; ***p<0.001). Gb3 signal, is expressed in cerebellum neurons independently of the genotype, although it appears more intense in nontreated mice compared to 5 months old wild type mice. A partial decrease of signal intensity was observed, after 3 or 5 months, in mice treated at birth with scAAV9-PGK-GLA.

Figure S6 Treatment with scAAV9-PGK-GLA preserves body weight of adult FD mice in both sexes

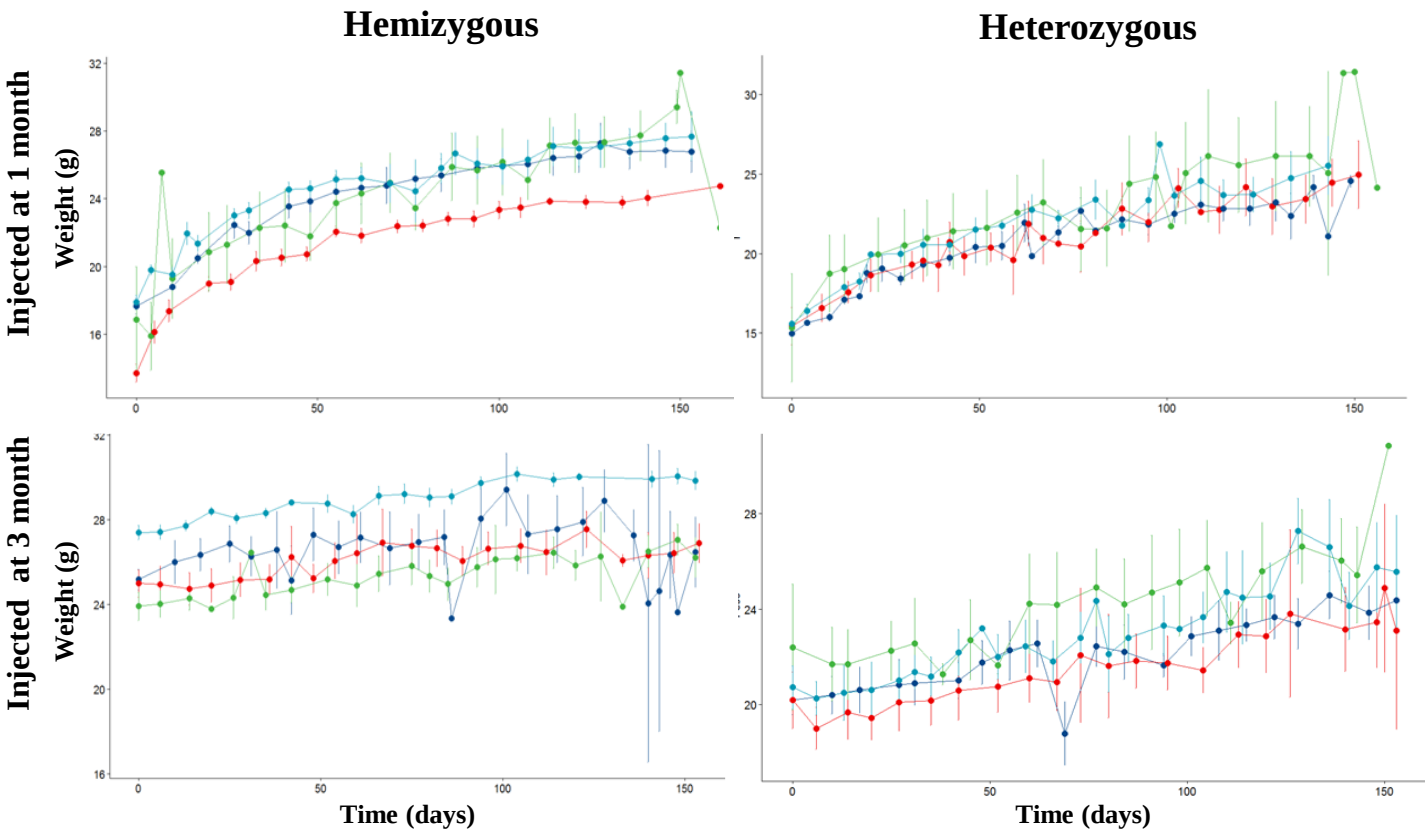

Body weight curves of FD mice treated or not and wild-type mice. Dark blue curve indicates mice injected with scAAV9-PGK-GLA at the dose of $6 \cdot 10^{13}$ vg/kg, red curve mice injected with scAAV9-PGK-GLA at the dose of $1.8 \cdot 10^{14}$ vg/kg, green non-injected hemizygous or heterozygous mice and light blue curve are sex-matched wild type mice (N=4). Error bars represents SEM. Statistic analysis was performed by Mixed ANOVA (Mauchly's test of sphericity and Greenhouse-Geisser) and determined that there are no significant differences in weight among the experimental groups.

Figure S7 The scAAV9-PGK-GLA drives the expression of α-GalA in heart, kidney, liver and plasma of FD mice.

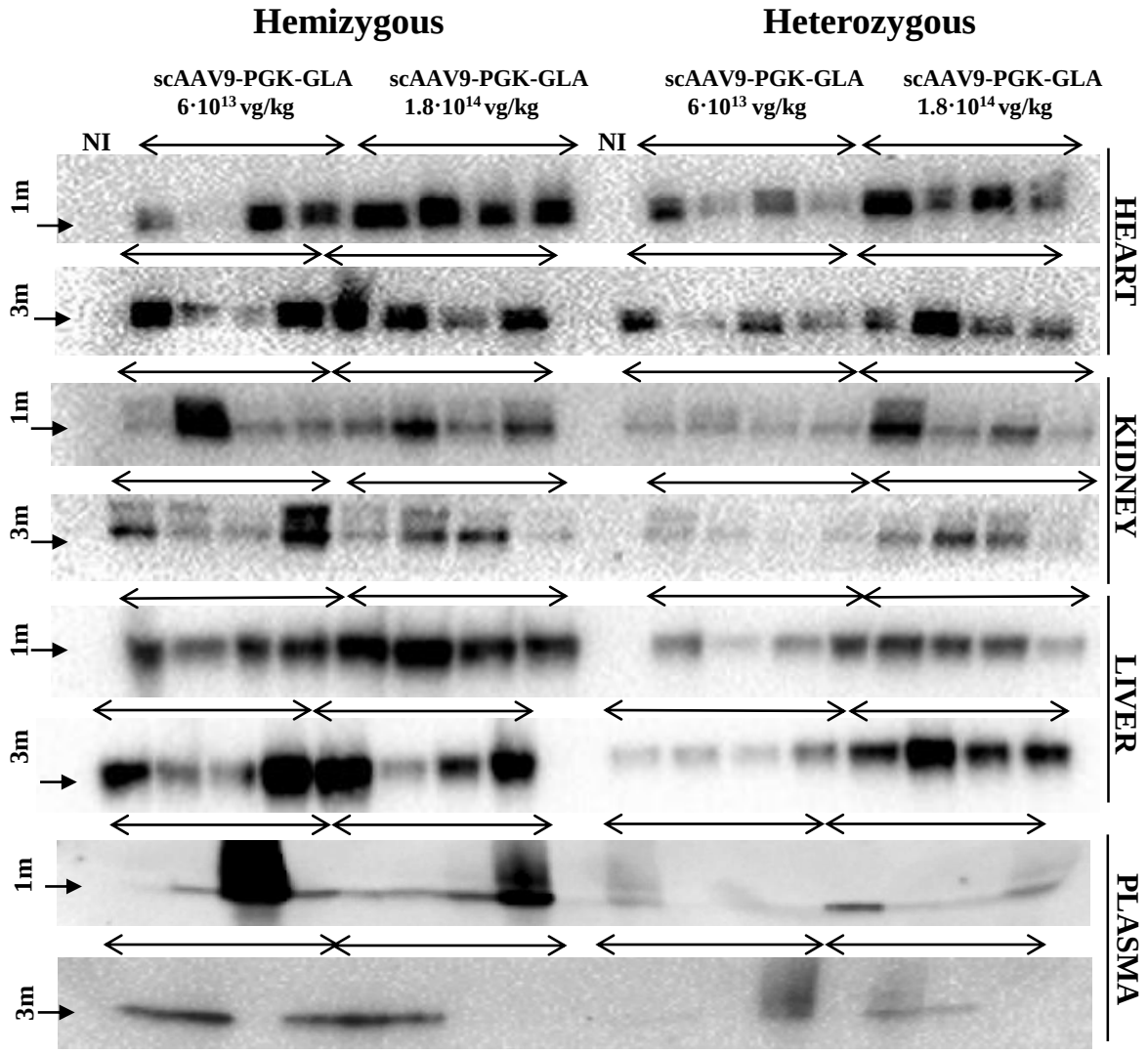

Western blot analysis of tissues (heart, kidney and liver) and plasma from 4 mice injected with scAAV9-PGK-GLA ($6 \cdot 10^{13}$ vg/kg or $1.8 \cdot 10^{14}$vg/kg) at either 1 month or 3 months (m) of age. Tissues were collected 5 months following the injection. A primary antibody, specific for the human isoform, was used to detect α-GalA (black arrow). NI represents genotype-matched noninjected animals.

Figure S8 Images of SDS-Page stain free gels of plasma and tissue lysates from FD mice, used to normalize western blot presented in Figure 4 and S7

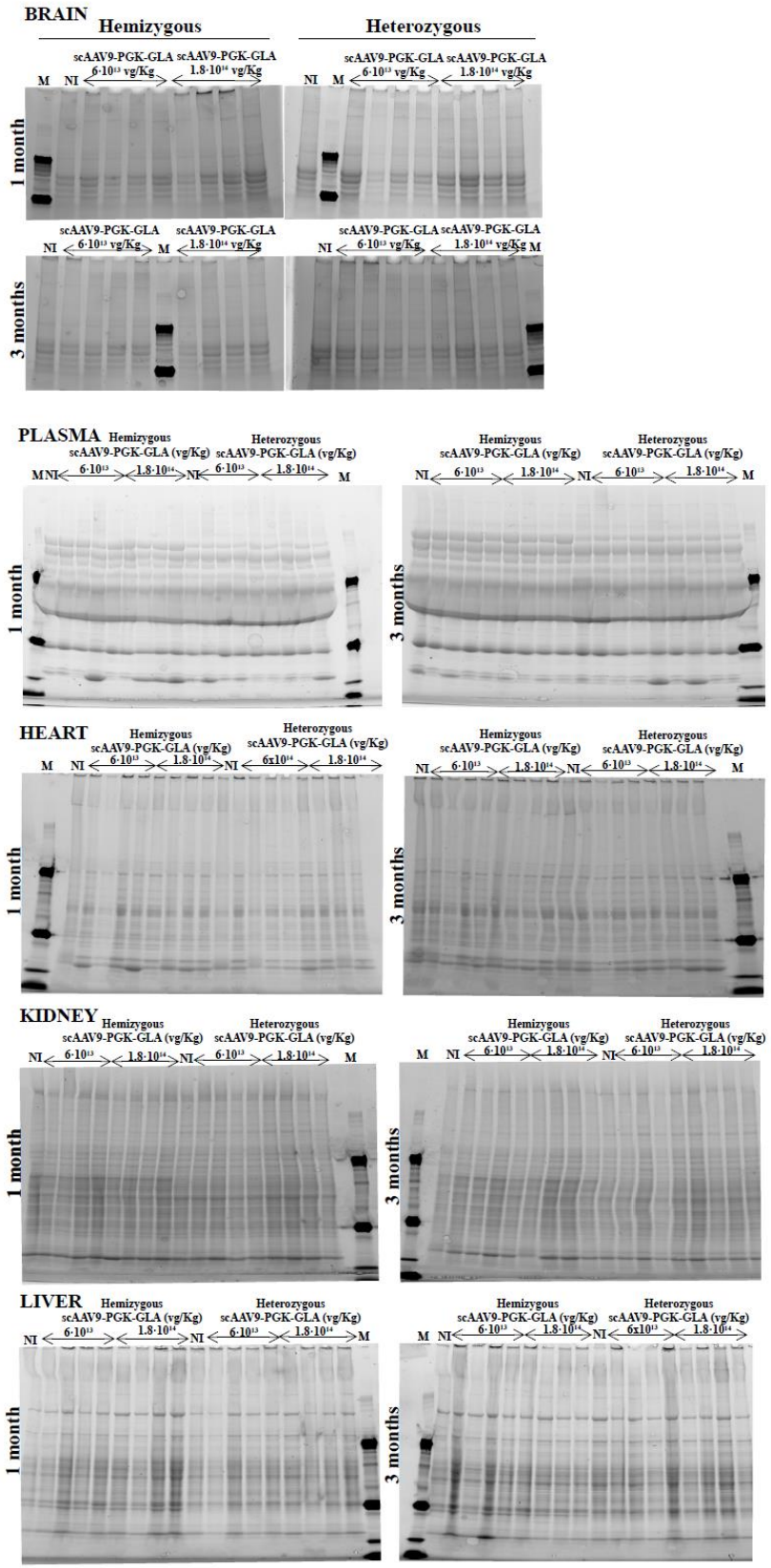

Stain-free gels (Biorad: #4568083, brain samples, and #5678081, other samples) were activated following manufacturer's indications and imaged before western blot to analyze α-GalA expression in each sample. These images were used to normalize α-GalA band intensity in each condition. The molecular weight marker (M) that is not visible in Figure S7 can be appreciated in these gels. NI represents genotype-matched noninjected animals.

Figure S9 Correlation between plasmatic levels of α-GalA and its activity

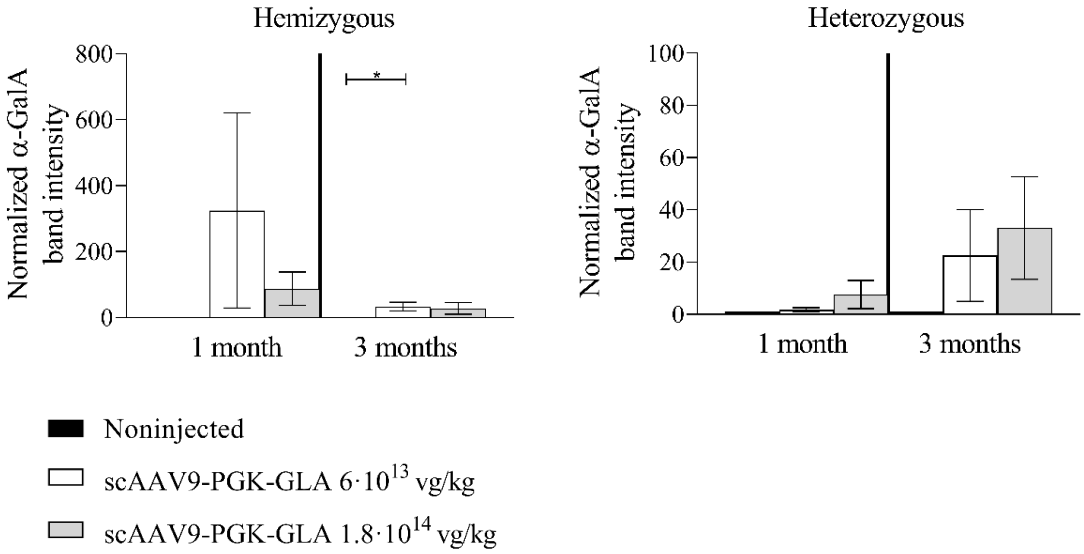

B

Activity/Amount of protein correlation	**Hemizygous**			
	Injected at 1 month		***Injected at 3 months***	
	$6{\cdot}10^{13}$ (vg /kg)	*$1.8{\cdot}10^{14}$ (vg /kg)*	*$6{\cdot}10^{13}$ (vg /kg)*	*$1.8{\cdot}10^{14}$ (vg /kg)*
Rho	1.00	0.80	1.00	1.00
Significance	0.33	0.2	0.08	0.08

Activity/Amount of protein correlation	**Heterozygous**			
	Injected at 1 month		***Injected at 3 months***	
	$6{\cdot}10^{13}$ (vg /kg)	*$1.8{\cdot}10^{14}$ (vg /kg)*	*$6{\cdot}10^{13}$ (vg /kg)*	*$1.8{\cdot}10^{14}$ (vg /kg)*
Rho	0.4	0.4	0.00	0.6
p value	0.6	0.6	1.00	0.4

(A) Histograms of western blot densitometric analysis of α-GalA in plasma, normalized to the corresponding total protein per lane (Figure S8) and reported to the intensity value obtained for the corresponding noninjected control. Error is expressed as SEM. Significance of the data, comparing each value with the value of the corresponding noninjected control was assessed by non-parametric t-test (*$p<0.05$; **$p<0.01$; ***$p<0.001$). (B) Correlation (Spearman's rank coefficient, Rho) between plasmatic levels of α-GalA reported in panel A and activity levels (Figure 5, plasma). Although values are not statistically significant (N=4), Rho coeficients show that values tend to correlate in the hemizygous injected mice, while this seems not to be the case in the heterozygous females, probably due to the contribution of the endogenous allele (not detected in WB) to the activity values.

Figure S10 Gb3 deposits are reduced in tissues from adult FD mice injected at 1 month of age with scAAV9-PGK-GLA

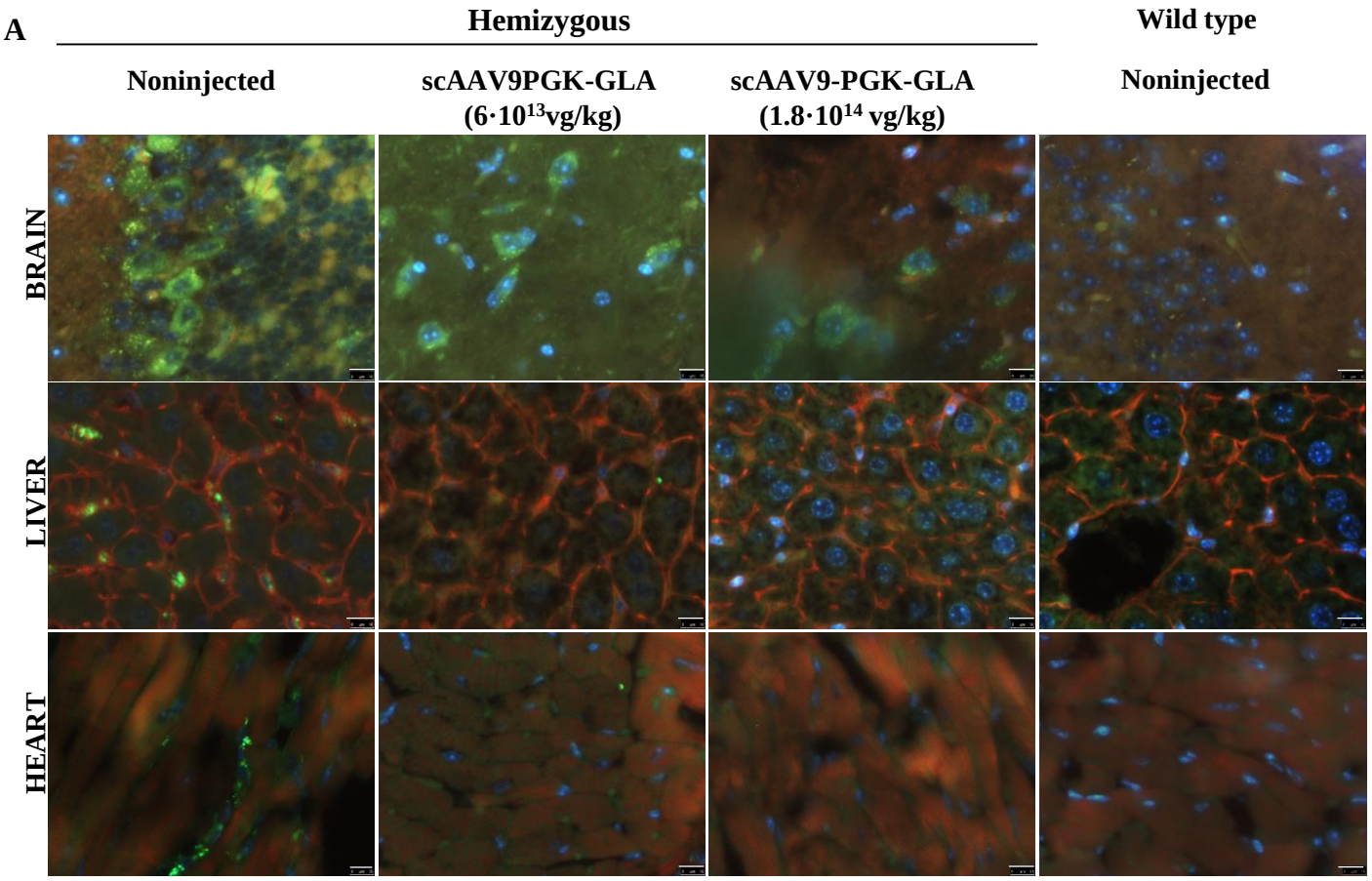

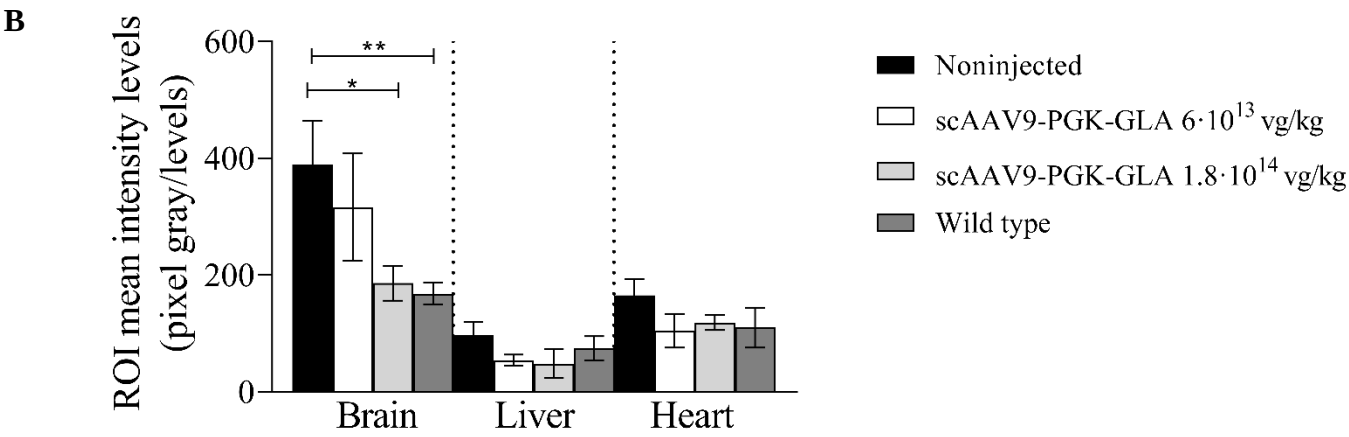

(A) Representative immunofluorescence images of Gb3 deposit in tissues (brain, liver, heart) from hemizygous FD mice injected with two doses of scAAV9-PGK-GLA at the age of 1 month and their age matched controls (noninjected hemizygous and wild type mice). Mice were sacrificed 5 months after injection. Gb3 was detected with a CD77-FITC antibody (green), polymerized actin was marked with Phalloidin-Rodhamine (red) and nuclei were stained with DAPI (blue). Scale bars =10 µm. (B) Histograms representing mean fluorescence in green channel (mean pixel intensity) as computed in different regions of interest, with constant area, defined for each images in Figure 7. Error is expressed as SEM. Significance of the data, comparing each value with the value of the corresponding non-injected control was assessed by nonparametric t-test (*p<0.05; **p<0.01; ***p<0.001). Gb3 deposits are present in intra-cardiac fibroblasts, cardiac epithelial cells, renal epithelial tubular cells, vascular smooth muscle cells, endothelial cells and CNS cells of non-injected hemizygous mice, while they are reduced in all these structures from mice treated with scAAV9-PGK-GLA at both doses.

Figure S11 Histograms relative to immunofluorescence intensity of Gb3 deposits shown in Figure 7.

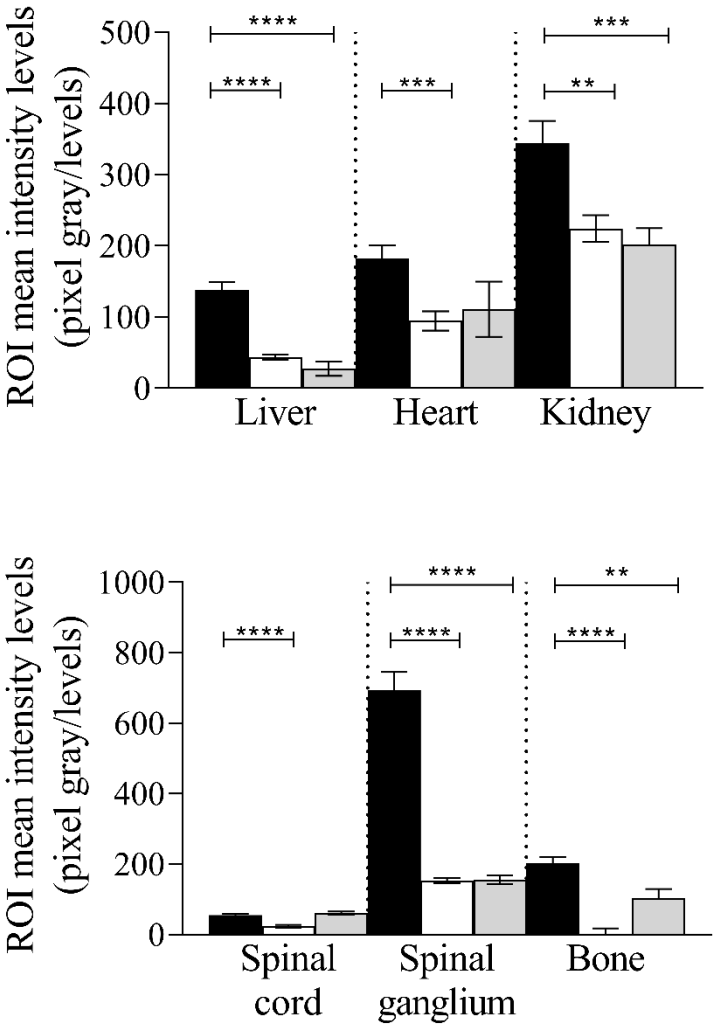

Histograms representing mean fluorescence in green channel (mean pixel intensity) as computed in different regions of interest with constant area defined for each images in Figure 7. Error is expressed as SEM. Significance of the data, comparing each value with the value of the corresponding noninjected control was assessed by nonparametric t-test (*$p<0.05$; **$p<0.01$; ***$p<0.001$).

Figure S12 Gb3 deposits were reduced in brain hippocampus and cortex from adult hemizygous mice injected at 3 months of age with scAAV9-PGK-GLA

A

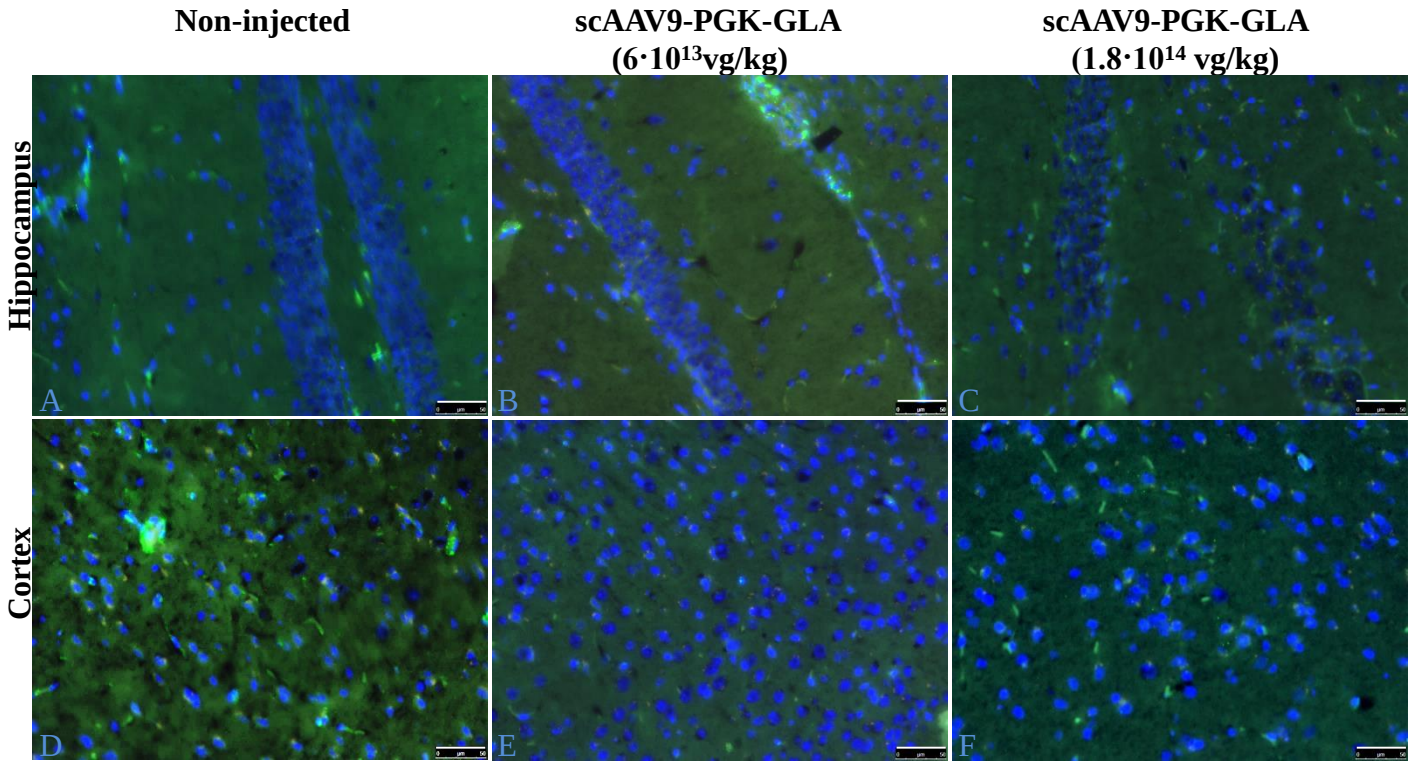

B

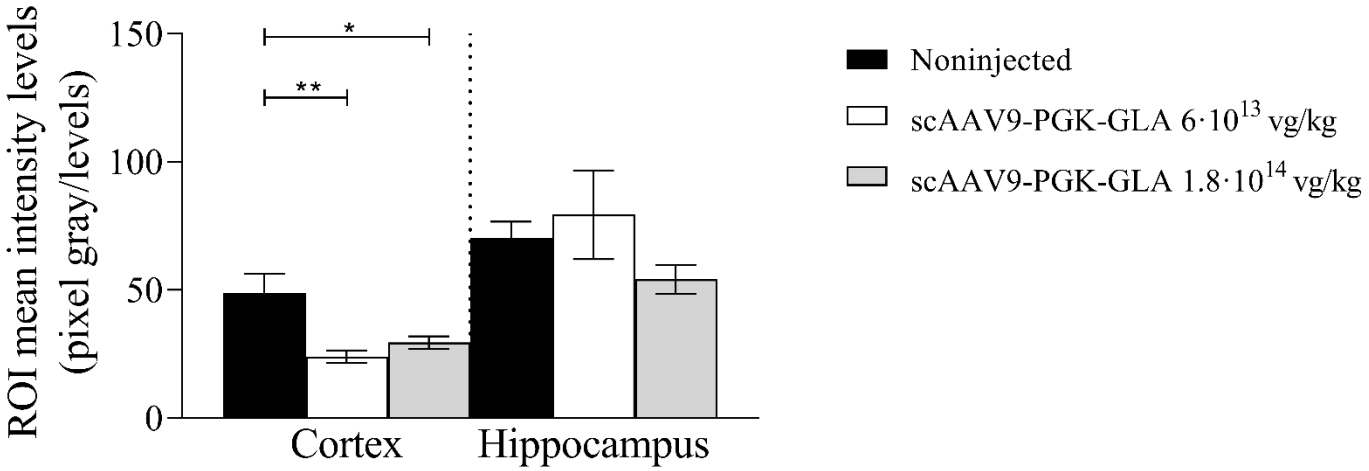

(A) Representative immunofluorescence images of Gb3 deposits in brain hippocampus and cortex from hemizygous FD mice injected with two doses of scAAV9-PGK-GLA at the age of 3 months and an age-matched non-injected control. Mice were sacrificed 5 months after injection. Gb3 was detected with a CD77-FITC antibody (green), polimeryzed actin was marked with Phalloidin-Rodhamine (red) and nuclei were stained with DAPI (blue). Scale bars = 75µm. Gb3 signal is detectable in blood vessels and CNS cells of the non-injected hemizygous mice (A and D), while it is less intense in the same structures from the mice treated with scAAV9-PGK-GLA at both doses (B, C, E, F). (B) Histograms representing mean fluorescence in green channel (mean pixel intensity) as computed in different regions of interest, with constant area, defined for each image. Error is expressed as SEM. Significance of the data, comparing each value with the value of the corresponding noninjected control was assessed by nonparametric t-test (*p<0.05; **p<0.01; ***p<0.001).

Table S1 Non-parametric assessment of variable correlation analyzed by calculating Spearman Coefficient (Rho).

Rho >0.7 indicates that variable are correlated and the coefficient is significant for $p<0.05$.

BRAIN treated at 1 month

Hemizygous scAA9-PGK_GLA $6\cdot10^{13}$ vg/kg				
Spearman Rho			*Virus titer*	*α-GalA activity*	*α-GalA expression*
	Virus titer	Rho	1.000	-0.600	1.000
		p	.	0.400	.
	α-GalA activity	Rho	-0.600	1,000	-0.600
		p	0.400	.	0.400
	α-GalA expression	Rho	1.000	-0.600	1.000
		p	.	0.400	.

Hemizygous scAA9-PGK_GLA $1.8\cdot10^{14}$ vg/kg				
Spearman Rho			*Virus titer*	*α-GalA activity*	*α-GalA expression*
	Virus titer	Rho	1.000	0.400	-0.400
		p	.	0.600	0.600
	α-GalA activity	Rho	0.400	1.000	-1.000
		p	0.600	.	.
	α-GalA expression	Rho	-0.400	-1.000	1.000
		p	0.600	.	.

Heterozygous scAA9-PGK_GLA $6\cdot10^{13}$ vg/kg				
Spearman Rho			*Virus titer*	*α-GalA activity*	*α-GalA expression*
	Virus titer	Rho	1.000	0.600	-0.400
		p	.	0.400	0.600
	α-GalA activity	Rho	0.600	1.000	-0.400
		p	0.400	.	0.600
	α-GalA expression	Rho	-0.400	-0.400	1.000
		p	0.600	0.600	.

Heterozygous scAA9-PGK_GLA1.$8\cdot10^{14}$ vg/kg				
Spearman Rho			*Virus titer*	*α-GalA activity*	*α-GalA expression*
	Virus titer	Rho	1.000	0.400	-0.800
		p	.	0.600	0.200
	α-GalA activity	Rho	0.400	1.000	-0.200
		p	0.600	.	0.800
	α-GalA expression	Rho	-0.800	-0.200	1.000
		p	0.200	0.800	.

BRAIN treated at 3 months

Hemizygous scAA9-PGK_GLA $6\cdot10^{13}$ vg/kg				
Spearman Rho			*Virus titer*	*α-GalA activity*	*α-GalA expression*
	Virus titer	Rho	1.000	-0.800	0.200
		p	.	0.200	0.800
	α-GalA activity	Rho	-0.800	1,000	-0.400
		p	0.200	.	0.600
	α-GalA expression	Rho	0.200	-0.400	1.000
		p	0.800	0.600	.

Hemizygous scAA9-PGK_GLA $1.8\cdot10^{14}$ vg/kg				
Spearman Rho			*Virus titer*	*α-GalA activity*	*α-GalA expression*
	Virus titer	Rho	1.000	-0.200	-1.000
		p	.	0.800	.
	α-GalA activity	Rho	-0.200	1.000	0.200
		p	0.800	.	0.800
	α-GalA expression	Rho	-1.000	0.200	1.000
		p	.	0.800	.

Heterozygous scAA9-PGK_GLA $6\cdot10^{13}$ vg/kg				
Spearman Rho			*Virus titre*	*α-GalA activity*	*α-GalA expression*
	Virus titer	Rho	1.000	0.800	-0.600
		p	.	0.200	0.400
	α-GalA activity	Rho	0.800	1.000	-0.800
		p	0.200	.	0.200
	α-GalA expression	Rho	-0.600	-0.800	1.000
		p	0.400	0.200	.

Heterozygous scAA9-PGK_GLA $1.8\cdot10^{14}$ vg/kg				
Spearman Rho			*Virus titer*	*α-GalA activity*	*α-GalA expression*
	Virus tier	Rho	1.000	-1.000	-0.500
		p	.	.	0.667
	α-GalA activity	Rho	-1.000	1.000	-0.400
		p	.	.	0.600
	α-GalA expression	Rho	-0.500	-0.400	1.000
		p	0.667	0.600	.

LIVER treated at 1 month

Hemizygous scAA9-PGK-GLA $6 \cdot 10^{13}$ vg/kg				
Spearman Rho		*Virus titer*	*α-GalA activity*	*α-GalA expression*
Virus titer	Rho	1.000	-0.200	0.000
	p	.	0.800	1.000
α-GalA activity	Rho	-0.200	1,000	0.400
	p	0.800	.	0.600
α-GalA expression	Rho	0.000	0.400	1.000
	p	1.000	0.600	.

Hemizygous scAA9-PGK-GLA $1.8 \cdot 10^{14}$ vg/kg				
Spearman Rho		*Virus titer*	*α-GalA activity*	*α-GalA expression*
Virus titer	Rho	1.000	-0.400	0.000
	p	.	0.600	1.000
α-GalA activity	Rho	-0.400	1.000	-0.200
	p	0.600	.	0.800
expression α-GalA	Rho	0.000	-0.200	1.000
	p	1.000	0.800	.

Heterozygous scAA9-PGK-GLA $6 \cdot 10^{13}$ vg/kg				
Spearman Rho		*Virus titer*	*α-GalA activity*	*α-GalA expression*
Virus titer	Rho	1.000	0.949	0.800
	p	.	0.051	0.200
α-GalA activity	Rho	0.949	1.000	0.949
	p	0.051	.	0.051
α-GalA expression	Rho	0.800	0.949	1.000
	p	0.200	0.051	.

Heterozygous scAA9-PGK-GLA $1.8 \cdot 10^{14}$ vg/kg				
Spearman Rho		*Virus titer*	*α-GalA activity*	*α-GalA expression*
Virus titer	Rho	1.000	-0.211	1.000
	p	.	0.789	.
α-GalA activity	Rho	-0.211	1.000	-0.211
	p	0.789	.	0.789
α-GalA expression	Rho	1.000	-2.11	1.000
	p	.	0.789	.

LIVER treated at 3 months

Hemizygous scAA9-PGK-GLA $6 \cdot 10^{13}$ vg/kg				
Spearman Rho		*Virus titer*	*α-GalA activity*	*α-GalA expression*
Virus titer	Rho	1.000	0.000	0.000
	p	.	1.000	1.000
α-GalA activity	Rho	0.00	1.000	0.000
	p	1.000	.	1.000
α-GalA expression	Rho	0.000	0.000	1.000
	p	1.000	1.000	.

Hemizygous scAA9-PGK-GLA $1.8 \cdot 10^{14}$ vg/kg				
Spearman Rho		*Virus titer*	*α-GalA activity*	*α-GalA expression*
Virus titer	Rho	1.000	-0.500	-1.000
	p	.	0.667	.
α-GalA activity	Rho	-0.500	1.000	0.316
	p	0.667	.	0.684
α-GalA expression	Rho	-1.000	0.316	1.000
	p	.	0.684	.

Heterozygous scAA9-PGK-GLA $6 \cdot 10^{13}$ vg/kg				
Spearman Rho		*Virus titer*	*α-GalA activity*	*α-GalA expression*
Virus titer	Rho	1.000	-0.800	-1.000
	p	.	0.200	.
α-GalA activity	Rho	-0.800	1.000	0.800
	p	0.200	.	0.200
α-GalA expression	Rho	-1.000	0.800	1.000
	p	.	0.200	.

Heterozygous scAA9-PGK-GLA $1.8 \cdot 10^{14}$ vg/kg				
Spearman Rho		*Virus titer*	*α-GalA activity*	*α-GalA expression*
Virus titer	Rho	1.000	-0.800	0.400
	p	.	0.200	0.600
α-GalA Activity	Rho	-0.800	1.000	0.000
	p	0.200	.	1,000
α-GalA Expression	Rho	0.400	0.000	1.000
	p	0.600	1.000	.

HEART treated at 1 month

Hemizygous scAA9-PGK-GLA 6·10[13] vg/kg						Hemizygous scAA9-PGK-GLA 1.8·10[14] vg/kg					
			Virus titer	*α-GalA activity*	*α-GalA expression*				*Virus titer*	*α-GalA activity*	*α-GalA expression*
Spearman Rho	*Virus titer*	Rho	1.000	0.400	0.400	**Spearman Rho**	*Virus titre*	Rho	1.000	-0.400	-0.200
		p	.	0.600	0.600			p	.	0.600	0.800
	α-GalA activity	Rho	0.400	1,000	-0.600		*α-GalA activity*	Rho	-0.400	1.000	-0.800
		p	0.600	.	0.400			p	0.600	.	0.200
	expression α-GalA	Rho	0.400	-0.600	1.000		*expression A-GalA*	Rho	-0.200	-0.800	1.000
		p	0.600	0.400	.			p	0.800	0.200	.

Heterozygous scAA9-PGK-GLA 6·10[13] vg/kg						Heterozygous scAA9-PGK-GLA 1.8·10[14] vg/kg					
			Virus titer	*α-GalA activity*	*α-GalA expression*				*Virus titer*	*α-GalA activity*	*α-GalA expression*
Spearman Rho	*Virus titer*	Rho	1.000	0.800	-0.800	**Spearman Rho**	*Virus titer*	Rho	1.000	1.000	-1.000
		p	.	0.200	0.200			p	.	.	.
	α-GalA activity	Rho	0.800	1.000	-0.400		*α-GalA activity*	Rho	1.000	1.000	-1.000
		p	0.200	.	0.600			p	.	.	.
	α-GalA expression	Rho	-0.800	-0.400	1.000		*α-GalA expression*	Rho	-1.000	-1.000	1.000
		p	0.200	0.600	.			p	.	.	.

HEART treated at 3 months

Hemizygous scAA9-PGK-GLA 6·10[13] vg/kg						Hemizygous scAA9-PGK-GLA 1.8·10[14] vg/kg					
			Virus titer	*α-GalA activity*	*α-GalA expression*				*Virus titer*	*α-GalA activity*	*α-GalA expression*
Spearman Rho	*Virus titer*	Rho	1.000	0.400	-0.400	**Spearman Rho**	*Virus titer*	Rho	1.000	0.800	0.600
		p	.	0.600	0.600			p	.	0.200	0.400
	α-GalA activity	Rho	0.400	1,000	-0.400		*α-GalA activity*	Rho	0.800	1.000	0.800
		p	0.600	.	0.600			p	0.200	.	0.200
	α-GalA expression	Rho	-0.400	-0.400	1.000		*α-GalA expression*	Rho	0.600	0.800	1.000
		p	0.600	0.600	.			p	0.400	0.200	.

Heterozygous scAA9-PGK-GLA 6·10[13] vg/kg						Heterozygous scAA9-PGK-GLA 1.8·10[14] vg/kg					
			Virus titer	*α-GalA activity*	*α-GalA expression*				*Virus titer*	*α-GalA activity*	*α-GalA expression*
Spearman Rho	*Virus titer*	Rho	1.000	-0.800	-0.400	**Spearman Rho**	*Virus titer*	Rho	1.000	-0.200	0.200
		p	.	0.200	0.600			p	.	0.800	0.800
	α-GalA activity	Rho	-0.800	1.000	0.000		*α-GalA activity*	Rho	-0.200	1.000	-1.000
		p	0.200	.	1.000			p	0.800	.	.
	α-GalA expression	Rho	-0.400	0.000	1.000		*α-GalA expression*	Rho	0.200	-1.000	1.000
		p	0.600	1.000	.			p	0.800	.	.

KIDNEY treated at 1 month

Hemizygous scAA9-PGK-GLA 6·10[13] vg/Kg					Hemizygous scAA9-PGK-GLA 1.8·10[14] vg/Kg				
Spearman Rho			*Virus titer*	*α-GalA activity*	*α-GalA expression*	Spearman Rho		*Virus titer*	*α-GalA activity*	*α-GalA expression*
	Virus titer	Rho	1.000	0.200	0.400		*Virus titer*	Rho	1.000	-0.400	-0.600
		p	.	0.800	0.600			p	.	0.600	0.800
	α-GalA activity	Rho	0.200	1,000	0.800		*α-GalA activity*	Rho	-0.400	1.000	-0.400
		p	0.600	.	0.200			p	0.600	.	0.600
	α-GalA expression	Rho	0.400	0.800	1.000		*α-GalA expression*	Rho	-0.600	0.400	1.000
		p	0.600	0.200	.			p	0.400	0.600	.
Heterozygous scAA9-PGK-GLA 6·10[13] vg/Kg						**Heterozygous scAA9-PGK-GLA 1.8·10[14] vg/Kg**					
Spearman Rho			*Virus titer*	*α-GalA activity*	*α-GalA expression*	Spearman Rho		*Virus titer*	*α-GalA activity*	*α-GalA expression*
	Virus titer	Rho	1.000	-0.800	1.000		*Virus titer*	Rho	1.000	-0.800	-0.800
		p	.	0.200	.			p	.	0.200	0.200
	α-GalA activity	Rho	-0.800	1.000	0.800		*α-GalA activity*	Rho	-0.800	1.000	0.400
		p	0.200	.	0.200			p	0.200	.	0.600
	α-GalA expression	Rho	-1.000	0.800	1.000		*α-GalA expression*	Rho	-0.800	0.400	1.000
		p	.	0.200	.			p	0.200	0.600	.

KIDNEY treated at 3 months

Hemizygous scAA9-PGK-GLA 6·10[13] vg/Kg					Hemizygous scAA9-PGK-GLA 1.8·10[14] vg/Kg				
Spearman Rho			*Virus titer*	*α-GalA activity*	*α-GalA expression*	Spearman Rho		*Virus titer*	*α-GalA activity*	*α-GalA expression*
	Virus titer	Rho	1.000	-0.600	-0.200		*Virus titer*	Rho	1.000	0.400	-0.800
		p	.	0.400	0.800			p	.	0.600	0.200
	α-GalA activity	Rho	-0.600	1.000	-0.200		*α-GalA activity*	Rho	0.400	1.000	0.200
		p	0.400	.	0.800			p	0.600	.	0.800
	α-GalA expression	Rho	-0.200	-0.200	1.000		*α-GalA expression*	Rho	-0.800	0.200	1.000
		p	0.800	0.800	.			p	0.200	0.800	.
Heterozygous scAA9-PGK-GLA 6·10[13] vg/Kg						**Heterozygous scAA9-PGK-GLA 1.8·10[14] vg/Kg**					
Spearman Rho			*Virus titer*	*α-GalA activity*	*α-GalA expression*	Spearman Rho		*Virus titer*	*α-GalA activity*	*α-GalA expression*
	Virus titer	Rho	1.000	-0.200	-0.800		*Virus titer*	Rho	1.000	0.800	0.000
		p	.	0.800	0.200			p	.	0.200	1.000
	α-GalA activity	Rho	-0.200	1.000	-0.400		*α-GalA activity*	Rho	0.800	1.000	-0.400
		p	0.800	.	0.600			p	0.200	.	0.600
	α-GalA expression	Rho	-0.800	-0.400	1.000		*α-GalA expression*	Rho	0.000	-0.400	1.000
		p	0.200	0.600	.			p	1.000	0.600	.

Table S2 IgG antibodies against α-GalA do not significantly affect activity in tissues from mice treated with scAAV9-PGK-GLA.

Summary of enzymatic activity and anti human α-GalA IgG antibody concentration in mice that produce antibodies against the enzyme. For each mouse producing antibodies against α-GalA, we calculated the percentage of their activity values in the indicated tissues, in reference to the average activity value of the whole group of animals (N=4) at the same age and with the same treatment (percentage indicated in brackets).

Mice ID	**Sex**	**Dose of the vector (vg/kg)**	**Age of injection (months)**	**[IgG] (ng/µl)**	**Mouse average value of α-GalA activity (nmol/h·mg)** *(% of average value of activity for the whole group)*					
					Plasma	**Liver**	**Heart**	**Kidney**	**Brain**	**Spleen**
B4	male	$6 \cdot 10^{13}$	1	13.34	3.55 *(12.3%)*	275.21 *(106.1%)*	132.22 *(102.7%)*	37.97 *(108.9%)*	13.58 *(136.5%)*	78.99 *(72.4%)*
G5	male	$1.8 \cdot 10^{14}$	1	12.61	33.39 *(117.6%)*	346.55 *(96.72%)*	321.80 *(76.1%)*	88.35 *(80.0%)*	22.93 *(81.5%)*	153.78 *(82.04%)*
D1	female	$6 \cdot 10^{13}$	1	16.23	3.4 *(69.7%)*	85.1 *(68.2%)*	135.75 *(91.1%)*	98.72 *(131.5%)*	46.64 *(96.4%)*	33.04 *(44.2%)*
X6	male	$6 \cdot 10^{13}$	3	2.96	2.47 *(4.9%)*	289.36 *(82.6%)*	103.42 *(28.9%)*	49.25 *(62.0%)*	15.35 *(130.3%)*	43.76 *(40%)*
J2	male	$1.8 \cdot 10^{14}$	3	7.83	0.38 *(0.48%)*	235.08 *(89.7%)*	167.49 *(126.7%)*	51.71 *(125.4%)*	6.92 *(62.1%)*	19.62 *(38.1%)*
J3	male	$1.8 \cdot 10^{14}$	3	28.6	1 *(1.3%)*	311.75 *(119.0%)*	226.66 *(171.4%)*	28.64 *(69.4%)*	13.91 *(124.8%)*	17.74 *(34.4%)*
W1	female	$6 \cdot 10^{13}$	3	40.62	3.51 *(12.3%)*	198.62 *(85.6%)*	137.21 *(112.5%)*	74.1 *(79.7%)*	73.6 (112.6%)	48.63 *(80.9%)*
I9	female	$1.8 \cdot 10^{14}$	3	15.01	5.83 *(37.4%)*	222.75 *(67.2%)*	120.81 *(74.7%)*	72.81 *(70.1%)*	86.07 *(124.6%)*	66.45 *(86.5%)*
Y7	female	$1.8 \cdot 10^{14}$	3	22.35	1.33 *(8.53%)*	264.18 *(79.8%)*	90.52 *(55.9%)*	55.63 *(53.5%)*	42.88 *(62.1%)*	49.08 *(63.9%)*